Polymer Nanocomposites for Photocatalytic Applications

Violeta Melinte * , **Lenuta Stroea** and **Andreea L. Chibac-Scutaru ***

Petru Poni Institute of Macromolecular Chemistry, 41 A Gr. Ghica Voda Alley, 700487 Iasi, Romania; elenah@icmpp.ro

* Correspondence: viomel@icmpp.ro (V.M.); andreea.chibac@icmpp.ro (A.L.C.-S.); Tel.: +40-232-217-454 (A.L.C.-S.)

check for
updates

Abstract: In the present comprehensive review we have specifically focused on polymer nanocomposites used as photocatalytic materials in fine organic reactions or in organic pollutants degradation. The selection of the polymer substrates for the immobilization of the active catalyst particles is motivated by several advantages displayed by them, such as: Environmental stability, chemical inertness and resistance to ultraviolet radiations, mechanical stability, low prices and ease availability. Additionally, the use of polymer nanocomposites as photocatalysts offers the possibility of a facile separation and reuse of the materials, eliminating thus the post-treatment separation processes and implicitly reducing the costs of the procedure. This review covers the polymer-based photocatalytic materials containing the most popular inorganic nanoparticles with good catalytic performance under UV or visible light, namely TiO_2, ZnO, CeO_2, or plasmonic (Ag, Au, Pt, Pd) NPs. The study is mainly targeted on the preparation, photocatalytic activity, strategies directed toward the increase of photocatalytic efficiency under visible light and reuse of the hybrid polymer catalysts.

Keywords: polymer composites; metal nanoparticles; photocatalytic efficiency; visible light

---

1. Introduction

Nanotechnology has experienced a fast development due to the variety of potential applications (industrial and military) that have attracted investments of billions of dollars in this research field. Over the last years, nanotechnology has gained a prominent role in our daily life, in 2014 being available over 1800 consumer products containing nanomaterials in their composition (e.g., paints, coatings, catalysts, cosmetics, some food products, food packaging, clothing, disinfectants, electronics) [1]. The considerable interest shown for the synthesis, characterization, and application of inorganic nanoparticles (NPs) is triggered by their remarkably different properties relative to those of the bulk counterparts, namely they have a larger surface area, higher reactive sites, and greater light absorption capacity. These properties of the inorganic NPs were exploited in the development of efficient photocatalysts mainly used for wastewater treatment [2], by degrading environmental pollutants [3,4], or by providing bactericidal activity [5,6]. However, despite their improved properties, the small size of the nanoparticles brings some issues regarding certain difficulties in their separation and reuse, and also possible risks to ecosystems and human health caused by the potential release of the nanoparticles into the environment [1]. An efficient approach to overcome the above drawback is to immobilize the nanosized particles onto a host material of larger size, finally a new type of material, namely a nanocomposite being formed. A variety of substrates appropriate for anchoring nanoparticles was reported in the literature, such as carbonaceous materials [7], silica [8], and polymers [9]. Particularly, the polymeric hosts are an attractive option for achieving this goal, partly because of their virtually unlimited architectural diversity, with elaborate and multifunctional surface chemistry, as well as of their good mechanical strength suitable for long-term applications. The main reason for this growing trend concerning polymer/inorganic functional materials derives from their ability to synergistically combine

the optical, electrical, and catalytic properties of nanoparticles with the flexibility and transparency of polymer matrices [10,11], which recommended them for various potential applications (in photonics, electronics, catalysis, or medicine). Since polymer-nanoparticle composites are promising candidates in the photocatalytic field, the adaptability of polymers as support for active photocatalytic nanoparticles (especially TiO_2) has been emphasized, underlying that besides the advantages listed above, they could also provide resistance against ultraviolet radiations or other environmental processes, high durability and stability, chemical inertness, and easy availability [12]. Additionally, the polymers facilitate the adsorption of the target organic molecules on their surface, improving the photocatalytic performance of the materials [13].

Photocatalysis can be applied for a variety of reactions, from mineralization of organic pollutants to fine organic processes, the great benefit of this method consisting of the direct conversion of light energy into chemical energy, thus reducing energy consumption or providing a green inexpensive approach to combating environmental pollution. Therefore, photocatalysis fulfills a part of the requirements of sustainable chemistry and green organic synthesis. So far, semiconductor materials are most used in photocatalysis [14,15] and TiO_2 is among the most preferred. Moreover, great interest was shown for the materials based on ZnO owing to its high spectral response in the UV region, which induced a very good photocatalytic performance, sometimes over TiO_2 [16,17]. However, slowly, conventional photocatalysts (TiO_2, ZnO) are replaced by other interesting metal oxides, cerium oxide nanoparticles (CeO_2 NPs) revealing a huge potential to provide sunlight active photocatalysts as one of the most reactive rare earth oxides that have a band gap similar to TiO_2 NPs (E_g = 3.19 eV). However, unlike TiO_2 with *d* electronic configuration, which permits the recombination of electron-hole pairs and may reduce the catalytic activity, CeO_2 has a *4f* electronic configuration that enhanced electron transfer from the adsorbed dye to the oxygen species [18]. Furthermore, in the literature are reported studies related to the good photocatalytic performance of noble metal nanoparticles, such as gold (Au), silver (Ag), palladium (Pd), or platinum (Pt). The materials incorporating them absorb both visible light mainly due to the localized surface plasmon resonance (LSPR) effect [19,20] and UV light due to interband electron transitions [19,21], making them suitable photocatalysts for sunlight irradiation.

This review aims to present the current state of the art in the field of polymer-based photocatalytic materials containing the most popular inorganic nanoparticles with good catalytic performance under UV or visible light, namely TiO_2, ZnO, CeO_2, or plasmonic (Ag, Au, Pt, Pd) NPs. The study is mainly focused on the preparation, photocatalytic activity, strategies directed toward the increase of photocatalytic efficiency under visible light and reuse of the hybrid polymer catalysts.

2. TiO_2 Nanoparticles

Since 1972, when Fujishima and Honda published their first report regarding the photoinduced decomposition of water on titanium dioxide (TiO_2) electrodes [22], many efforts have been dedicated to the investigation of TiO_2 photocatalytic properties and to the development of titanium dioxide catalysts with improved photocatalytic efficiency. TiO_2 is intensively studied in the literature as a photocatalyst due to its excellent properties, such as: Long term stability, low cost, non-toxic nature, chemical resistance, superior redox ability, and photoelectric properties [23–29]. Nevertheless, TiO_2 is an effective photocatalyst only in anatase form and only in UV light (3%–5% of sunlight) due to its band gap of 3.2 eV, which represents a serious drawback in the opportunity of employing sunlight as radiation source. Many research activities have been directed towards increasing the TiO_2 photocatalysts efficiency under visible light illumination (45%–50% of sunlight). Accordingly, some of the most favorable approaches used to attain this objective are doping, coupling, surface modification, or surface covering with other metal oxides [30], transitional metal ions [31,32], noble metals [33–36], and non-metals [37–39].

In order to eliminate the post-treatment separation processes of titanium dioxide catalyst and to provide the possibility of reusing the photocatalyst with minimal costs, the immobilization of titania on a wide variety of substrates was reported in the literature. Singh et al. [26] presented the

versatility of polymers as support for TiO_2 photocatalysts due to their several advantages such as flexible nature, low cost, resistance against ultraviolet radiations, high durability, chemical inertness, mechanical stability, and easy availability. In fact, in 2013 Singh et al. reported a comprehensive study in the field of polymer-based TiO_2 photocatalysts [26], so in the present review we cover studies related to polymer-supported titanium dioxide photocatalysts published in the literature after 2013. The photocatalytic activity of the final materials depends on the immobilization method of the active catalyst particles on the substrate, in the following the photocatalytic performance of different hybrid polymer-TiO_2 catalysts will be discussed.

### 2.1. TiO₂ Immobilized on the Surfaces of Polymer Substrates

Considering that for the beginning we will focus on TiO_2 anchored on various polymer matrices, it should be mentioned that the first report referring to the immobilization of TiO_2 photocatalyst on a polymeric substrate was made in 1995 by Tennakone [40] and presented the use of titania supported on polythene films as photocatalyst for phenol degradation, the decomposition degree being 50% after 2.5 h exposure to sunlight. Since then, more diverse and complex polymeric structures employed as substrates for TiO_2 catalysts were studied in the literature.

One of the methods commonly used for TiO_2 immobilization consists in the modification of polymer surface to attain an improved affinity for TiO_2. Plasma treatment has great potential for this purpose and has been used to attach TiO_2 on different substrates. Some commercially available polymeric films, namely, poly (vinyl chloride) (PVC), poly (methyl methacrylate) (PMMA), and polystyrene (PS) were subjected to low pressure (LPP) and atmospheric pressure (APP) plasma action so that the surface properties were modified [41]. After pre-treatment, three layers of TiO_2 were deposited on the polymeric films by the dip coating process, the adhesion of TiO_2 to the polymers was improved due to the generation of roughness and specific polar functional groups on the polymer surfaces. TiO_2 loading was higher and more homogeneous in the plasma treated samples compared to the untreated ones. The TiO_2-containing materials were tested as photocatalysts under UV irradiation for trichloroethylene photodegradation in air. The best results were achieved for the films treated with low pressure plasma, the photodegradation efficiency being 15% higher in the case of PS-LPP-Ti as compared to the untreated sample PS-Ti and with 40% higher for PVC-LPP-Ti relative to PVC-Ti [41]. Another study presents the development of TiO_2 coatings on polypropylene (PP) foil pre-treated with low temperature oxygen plasma [42]. The exposure of PP film to low temperature oxygen plasma generated oxygen-containing groups on the polymer surface, and after the dip-coating procedure in TiO_2 nanoparticles aqueous solution, a compact TiO_2 coating was obtained on the polymeric surface. The adhesion between the inorganic oxide and the PP surface was very good due to the strong electrostatic interactions and the formation of covalent bonds (Ti-O-C). In order to achieve films with photocatalytic activity under visible light, the titania-PP film was impregnated with the solution of various organic ligands (catechol, 2,3-naphthalenediol, pyrogallol, and rutin) that form surface Ti (IV) charge transfer complexes, which ensure an effective photoinduced charge separation and finally leads to redox reactions for pollutant degradation. Of all the titanium dioxide sensitized coatings, the one modified with catechol proved to be the most photoactive under visible irradiation, indicating that it can successfully participate in photocatalytic reactions [42].

A good approach to modify the polymeric surfaces for TiO_2 NPs immobilization is to graft the polymer with compounds bearing functional units ($-NH_2$, -COOH, etc.) capable to interact with the hydroxyl groups from titania. On a polyethersulfone microfiltration membrane (PES), TiO_2 NPs were immobilized using the dip-coating method by three different paths: (i) Standard method—TiO_2 NPs were attached to the membrane at 210 °C, (ii) ultrasound method—TiO_2 NPs in suspension were treated with ultrasound to avoid agglomeration of the nanoparticles and after they were immobilized on the membrane at 210 °C (210 °C + US), (iii) membrane pre-modification—membrane was modified with polyacrylic acid (PAA) by electron beam irradiation in order to generate carboxyl groups (COOH) on the membrane surface and subsequently TiO_2 NPs were anchored on the membrane at 210 °C

(210 °C + COOH) [43]. These modification methods led to a better and homogenous coverage of the membrane with TiO_2 nanoparticles, the amount of titanium depending on the method used for the immobilization of nanoparticles, 3% for standard, 9% for 210 °C + US and 14% for 210 °C + COOH. The authors demonstrated by the stability test that TiO_2 NPs were strongly bound to the membrane and they investigated the photocatalytic activity of the samples in degrading methylene blue (MB) and carbamazepine. Regarding the MB photodegradation, the evaluated samples did not display very different photocatalytic activity, the rate constant being around 11×10^{-2} min^{-1}, even if TiO_2 NPs distribution was increased in 210 °C + US and 210 °C + COOH samples. By testing the photocatalytic activity for carbamazepine degradation, the photodegradation efficiency decreased in series 210 °C + US > 210 °C + COOH > 210 °C. Additionally, it has been demonstrated that the TiO_2 membrane can be reused without loss of performance for up to nine cycles [43].

Yang et al. fabricated a TiO_2 photocatalyst by growing TiO_2 NPs with high crystallinity on the surface of a pretreated poly (phenylene sulfide) (PPS) porous membrane via in situ hydrothermal process [44]. Firstly, the microporous membrane was pretreated with HNO_3, thus partially oxidizing the -S- bond to -SO- bond. Subsequently, the hydrolysis products of tetrabutyl titanate were attached to the membrane by strong electrostatic interactions and formed nucleation sites where TiO_2 particles were developed leading to the TiO_2@PPS membrane (Figure 1a). The TiO_2@PPS membrane had an efficient photocatalytic activity in the degradation process of some dyes (rhodamine B—RhB, methyl orange—MO, methylene blue—MB) under visible irradiation. The catalytic activity in visible light was triggered by the interactions between TiO_2 and the conjugated structure of the polymeric membrane, which decrease the band gap and the electron/hole recombination rate for TiO_2 particles, thus assisting efficient separation of electron-hole pairs and improving the visible-light activity (Figure 1b). After 90 min of visible irradiation in the presence of TiO_2@PPS catalyst, the photocatalytic degradation efficiencies for RhB, MB, and MO are 99.56%, 98.05%, and 93.18%, with the rate constants (k) of the degradation 4.58, 3.64, and 2.53×10^{-2} min^{-1}, respectively.
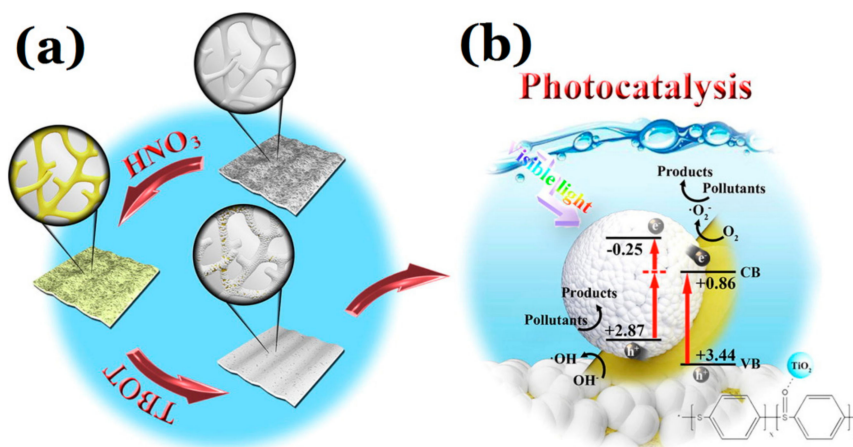
Figure 1. Schematic illustration of the preparation of TiO_2@PPS microporous membrane (**a**) and the probable photocatalytic mechanism of the TiO_2@PPS membrane (**b**). Reproduced by permission of Elsevier from [44].

Nowadays, the availability of synthetic polymers derived from oil, gas, and carbon (non-renewable sources) is decreasing, so the scientific community is looking for cheaper and more readily accessible alternatives, such as biopolymers derived from raw materials. For example, xylan is a biopolymer with excellent film forming properties used for the preparation of a xylan/polyvinyl alcohol (PVA)/TiO_2 composite, PVA being employed as a crosslinking agent and xylan as a template so that the TiO_2 particles homogeneously adhere to the composite surface [45]. The xylan/PVA/TiO_2 composite had a satisfactory photocatalytic performance under visible irradiation in the photodegradation of ethyl violet and Astrazon Brilliant Red 4G dyes. The decolorization rates of ethyl violet and astrazon brilliant

red 4G dyes were 93.65% and 92.71%, respectively after 60 min of visible irradiation at a catalyst dosage of 100 mg/L. This is the optimum concentration of catalyst for best results in photocatalysis, above this concentration a decrease of dyes bleaching rate occurred. Moreover, the xylan /PVA/TiO$_2$ composite showed good performance in phenol degradation, in 60 min being decomposed 93% phenol [45]. An interesting approach was to fabricate a photocatalyst by stacking a layer of Au@TiO$_2$ nanostructures on a chitosan fiber substrate [46]. Due to the surface plasmon resonance effect of Au, the plasmonic fiber exhibited catalytic activity in visible light in the degradation of various pollutants (MB, carbofuran—CBN, and metronidazole—MNZ) and for the reduction of chromium (VI) to Cr(III). The plasmonic fiber degraded 98.8% MB in only 12 min of irradiation (k = 0.85 × 10^{-2} min^{-1}) using low catalyst dosage (3 × 10^{-3} g/L), its catalytic performance being quite stable even after eight runs (loss ~ 4.1%). In the case of CBN and MNZ, the reaction times were longer, namely 130 min (k = 1.05 × 10^{-2} min^{-1}) and 260 min (k = 0.9 × 10^{-2} min^{-1}), respectively. The results were improved by adding H$_2$O$_2$ in the systems, when the photodegradation degree of CBN reached 98.3% (k = 3.06 × 10^{-2} min^{-1}) and 96% for MNZ (k = 2.17 × 10^{-2} min^{-1}). The plasmonic fiber photocatalyzed the reduction reaction of Cr(VI) to Cr(III) within 21 min visible irradiation, in the presence of citric acid (pH = 1) with an efficiency of 98.9% [46]. On the same principle as before, another photocatalyst was developed by covering the surface plasma pretreated cotton fabrics with polyaniline/TiO$_2$ (PANI/TiO$_2$) co-doped with sulfosalicylic acid (SSA) and sodium dodecyl benzene sulfonate (SDBS) through one-step in situ polymerization [47]. The oxygen plasma treatment was used to introduce more –OH groups on the surface of cotton fibers, while SSA and SDBS were used as doping acids to increase the photocatalytic activity. PANI/TiO$_2$/cotton composite fabric exhibited good photocatalytic performance under simulated sunlight irradiation for RhB degradation, the total efficiency being 87.6% after 180 min of irradiation [47].

2.2. TiO$_2$ Immobilized in Polymer Substrates

In many studies, TiO$_2$ was embedded in various polymer matrices and further used in photocatalytic applications. A simple polymer substrate utilized for TiO$_2$ immobilization was recycled poly (ethylene terephthalate) (PET). The PET/TiO$_2$ nanocomposite films with different TiO$_2$ amounts (10, 30, and 47 wt % TiO$_2$) were prepared by the phase inversion method [48]. The achieved films showed photocatalytic activity in the degradation of a mixture of antibiotics (isoniazid, metronizadole, sulfadiazine, sulfamethoxazole, trimethoprim, norfloxacin, moxifloxacin, and lincomycin) under simulated solar irradiation. In the first cycle of use, the photocatalytic efficiency was better for the composites with a higher quantity of TiO$_2$. However, in the second run, PET-30 wt % TiO$_2$ and PET-47 wt % TiO$_2$ did not have reproducible results, because the active oxidative species produced by TiO$_2$ particles during the first catalytic cycle attacked the PET chains, breaking them and the TiO$_2$ NPs were leached from the polymeric substrate. On the other hand, PET-10 wt % TiO$_2$ composite film had good stability even after five cycles of utilization. PET-10 wt % TiO$_2$ catalyst degraded almost totally some of the antibiotics after 2 h of irradiation: Lincomycin (k = 2.4 × 10^{-2} min^{-1}), moxifloxacin (k = 6.5 × 10^{-2} min^{-1}), isoniazid (k = 2.6 × 10^{-2} min^{-1}), metronidazole (k = 3.7 × 10^{-2} min^{-1}), and norfloxacin (k = 6.7 × 10^{-2} min^{-1}). The rest of the compounds from the mixture required longer reaction times (6 h of irradiation) for their photodecomposition: Trimethoprim (90%, k = 0.7 × 10^{-2} min^{-1}), sulfadiazine (93%, k = 0.9 × 10^{-2} min^{-1}), and sulfamethoxazole (98%, k = 1.5 × 10^{-2} min^{-1}). The catalyst was also efficient in degrading the target compounds in wastewater matrix, but the process rates were lower [48]. In another study, TiO$_2$ NPs were embedded in fluoropolymers, the photocatalytic coating being realized from a layer of TiO$_2$-containing perfluorosulfonic acid polymer on a layer of perfluorinated amorphous polymer [49]. The designed material proved to be an efficient system for the gas-phase degradation of volatile organic compound (VOC) under UV exposure, the photodecomposition of pentane (k = 10 × 10^{-6} s^{-1}), methanol (k = 144 × 10^{-6} s^{-1}), 2-propanol (k = 473 × 10^{-6} s^{-1}), toluene (k = 11 × 10^{-6} s^{-1}), dichloromethane (k = 6.6 × 10^{-6} s^{-1}), and pyridine (k = 46 × 10^{-6} s^{-1}) in dry condition was being followed. The performed studies have shown that the

photocatalytic performance of the material depends on the humidity conditions and on the interactions between the ionomeric layer of the coating and the pollutants [49].

Zhang's group incorporated different amounts of TiO_2 NPs (10–80 wt %) in conjugated microporous polymer obtained by a Sonogashira crosscoupling reaction of 1,3,5-triethynylbenzene as crosslinker and 4,7-dibromo-2,1,3-benzothiadiazole as comonomer [50]. The hybrid materials have been successfully used as photocatalysts for oxidative coupling of benzylamines under visible light irradiation at room temperature, the highest conversion (98%) being obtained for the material containing 20 wt % TiO_2 NPs. For this reaction, TiO_2 NPs alone were inactive, so the combination of organic/inorganic semiconductor enhanced the photoinduced charge separation and therefore increased the photocatalytic efficiency [50]. TiO_2-poly (vinylidene fluoride) (PVDF)/ poly (methyl methacrylate) (PMMA) nanocomposite membranes with a porous and sponge-like structure and different amounts of TiO_2 (0.12, 0.25, and 0.5 wt %) were prepared by phase inversion method [51]. The hybrid materials exhibited photocatalytic activity in MB degradation under UV irradiation, so after 330 min 86% MB was removed with M-0.12 wt % TiO_2 (k = 0.55×10^{-2} min^{-1}), 95% MB with M-0.25 wt % TiO_2 (k = 0.84×10^{-2} min^{-1}) and 99% MB with M-0.5 wt % TiO_2 (k = 0.17×10^{-2} min^{-1}), MB photodegradation increasing with the content of TiO_2 NPs enclosed in the membrane.

An unusual approach was to incorporate the TiO_2 gel domain without calcination in the reverse micelle structure of poly (styrene-block-acrylic acid) (PS-*b*-PAA) [52]. The reverse micelles consisting of hydrophilic core (PAA) and hydrophobic corona (PS) were the nano-template for TiO_2 gel synthesis and will preserve their structure with TiO_2 domain inside even after drying. The photocatalytic activity of the micellar systems was tested in MB degradation in water under visible light irradiation and it was observed that the photodegradation of MB is mainly influenced by the polymer chain length and the PAA/PS molar ratio. Initially, the MB is absorbed at the chains and only the absorbed MB existing in the vicinity of the gel is photodegraded. The best photocatalytic activity was achieved in the presence of PS$_{330}$-*b*-PAA$_{34}$ containing TiO_2 gel, when the MB decomposition was accomplished within 240 min with a rate constant k = 0.17×10^{-2} min^{-1}. The catalytic activity was considerably improved by loading copper phthalocyanine in the reversible micelle, thus the reaction time was reduced to 180 min and the rate constant was about three times higher (k = 0.6×10^{-2} min^{-1}). This fact has been attributed to an efficient charge separation at the interface between TiO_2 and copper phthalocyanine, created under visible light irradiation. Moreover, the photocatalytic system presented a good stability and has the potential to be reused [52].

Our group has developed TiO_2 hybrid composites based on photocrosslinked matrices, since the utilization of photocuring technology (photopolymerization/photocrosslinking) for the preparation of polymeric materials is a convenient, very simple, non-invasive technique that does not require expensive devices and long reaction times [53]. In a first report, thin composite films were obtained by the photopolymerization of an acrylic monomer mixture, namely an acidic urethane dimethacrylate based on poly(ethylene glycol) as the major component (80 wt %), 3-(trimethoxysilyl)propyl methacrylate as the inorganic component (10 wt %) able to create the silsesquioxane sequences and 3-(acryloyloxy)-2-hydroxy-propyl methacrylate as a coupling agent (10 wt %) to generate interactions between the organic and the inorganic phases [53]. Titanium butoxide derivative was added to the mixture before photopolymerization in different gravimetric ratios (5–20 wt %). In the second stage, the films were kept in a chamber with constant humidity, so that the sol-gel process took place and finally the silsesquioxane sequences were formed along the main macromolecular chain and the titania domains inside the polymer substrate. The obtained TiO_2/SiO_2 phases were mainly amorphous and, in order to attain photocatalytic materials with adequate performance, noble metal NPs (Ag/Au) were in situ photogenerated in the polymer network during the UV-curing, simultaneously with the photopolymerization process. The polymeric films exhibited good catalytic activity for phenol derivatives (phenol and *o*-nitro-phenol) photodegradation under low intensity UV irradiation (to simulate the UV radiation from solar light), the photocatalytic performance being improved by increasing the TiO_2 content in the films and also by the presence of Ag/Au NPs. The photodegradation

degrees and the rate constants after 70 min of UV irradiation for phenol are as follows: S1 (5 wt % TiBu)—56% and k = 1.14×10^{-2} min^{-1}, S2 (10 wt % TiBu)—63% and k = 1.45×10^{-2} min^{-1}, S3 (20 wt % TiBu)—72% and k = 1.65×10^{-2} min^{-1}, S2-Ag (10 wt % TiBu and 1 wt % Ag NPs)—83% and k = 2.43×10^{-2} min^{-1} and S2-Au (10 wt % TiBu and 1 wt % Au NPs)—77% and k = 2.12×10^{-2} min^{-1}. The photodegradation parameters for *o*-nitro-phenol decomposition are similar to those determined for phenol. This study underlined that, even in the absence of the crystalline TiO_2 phase, but in appropriate combination with other conducting elements (SiO_2 phase and Ag/Au NPs), the proposed materials acted as good catalyst capable to eliminate phenol derivatives from the system nearly completely after 350 min of UV irradiation [53].

In a subsequent study, within a photopolymerizable urethane dimethacrylate (polytetrahydrofuran-urethane dimethacrylate, PTHF-UDMA) we enclosed 10 wt % TiO_2 NPs (nanocrystalline anatase phase) pure or in different blends, namely: TiO_2 NPs with Si–O–Si sequences (TiO_2/SiO_2), TiO_2 with maghemite nanoparticles (TiO_2/Fe_2O_3), and TiO_2 with Si–O–Si and maghemite ($TiO_2/SiO_2/Fe_2O_3$) [54]. After the photopolymerization procedure (5 min under UV irradiation), four different types of hybrid cross-linked films (S1–S4) were obtained, which exhibited catalytic activity in the degradation of hydroxybenzene compounds (phenol, hydroquinone, and dopamine) upon UV and visible light exposure. The degradation of hydroxybenzene derivatives under UV irradiation (250 min) is more efficient for the films containing TiO_2 NPs combined with other inorganic components, according to series S1 (TiO_2 NPs) < S2 (TiO_2/SiO_2) < S3 (TiO_2/Fe_2O_3) < S4 ($TiO_2/SiO_2/Fe_2O_3$) since the presence of the other semiconductors synergistically improved the charge separation. The photodegradation degree varied between 77%–99% and the rate constants k were in the range $0.72 \div 2.38 \times 10^{-2}$ min^{-1}. In visible light, only S3 and S4 hybrid films containing maghemite NPs behaved as active catalysts, since Fe^{3+} cations extended the UV-vis absorption of TiO_2 to the visible domain. Phenol and dopamine model pollutants were degraded after 250 min visible irradiation in proportion of ~80%–83% (k = 1.8×10^{-2} min^{-1}) and 89%–95% (k = $0.85 \div 1.15 \times 10^{-2}$ min^{-1}), respectively. The hydroquinone photodecomposition process was faster in visible light, so after 90 min of irradiation, the compound was completely removed and the rate constant was k = 8.5×10^{-2} min^{-1} [54].

Research in this field has been continued in our group and, therefore, in order to attain a covalent attachment of inorganic TiO_2 NPs inside the photocrosslinked coatings, preventing thus their inactivation by agglomeration or their diffusion from the polymer matrix, the surface of TiO_2 NPs was functionalized with photopolymerizable acrylic groups [55]. The hybrid polymeric films (F-0, F-2, F-5, and F-10) were prepared by the photopolymerization of an urethane dimethacrylate monomer mixture in which various amounts of functionalized TiO_2 NPs (between 2–10 wt %) were introduced. Simultaneously with the photopolymerization process, in F-10 formulation, Ag/Au NPs were in situ photogenerated from the corresponding metal salts (2 wt % $AgNO_3/AuBr_3$), the schematic process for the preparation of the hybrid composites (F-10-Ag, F-10-Au) being illustrated in Figure 2.
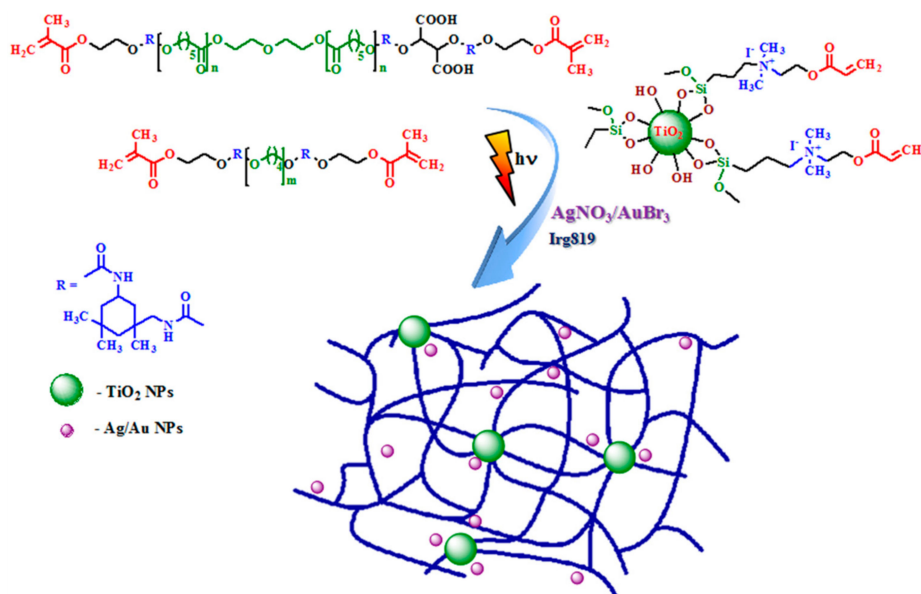
Figure 2. Representation of the formation of hybrid polymer networks containing TiO$_2$ NPs functionalized with photopolymerizable acrylic groups. Reproduced by permission of John Wiley and Sons from [55].

The catalytic activity of the hybrid materials under UV irradiation against phenol is quite good for this class of materials with a high degree of cross-linking and without a porous structure. The photocatalytic performance was enhanced by increasing the loading of TiO$_2$ NPs in the polymeric matrix and also by the presence of noble metal nanoparticles (Ag/Au), the best results in phenol degradation under UV irradiation being obtained for F-10-Au film (87.8%, k = 1.34×10^{-2} min^{-1}). Under visible light exposure, only the hybrid composites containing Ag/Au NPs displayed photocatalytic activity for phenol decomposition, the degradation degree (89%) and the rate constant (k = 1.05×10^{-2} min^{-1}) being almost the same for F-10-Au and F-10-Ag composites. The good catalytic activity of plasmonic-TiO$_2$ materials under UV and visible light and the fact that they can be reused for multiple runs (the composites have been tested for five cycles without significant loss of performance) make them promising candidates for use as photocatalyst in real sunlight. The polymeric films incorporating Ag/Au NPs besides TiO$_2$ NPs proved to be very good catalysts for organic dyes degradation, removing entirely Congo Red from an aqueous solution after 450 min of visible irradiation [55].

Another research group incorporated TiO$_2$ NPs (10 wt %) into a commercially available acrylate, namely, poly (ethylene glycol) diacrylate, by photopolymerization method (700 ms at 240 mW/cm^2), resulting in a PEGDA/TiO$_2$ composite film with homogeneous wrinkled structure (Figure 3) [56]. The hybrid film had a very good adsorption capacity of organic dyes (Congo Red was selected as a model pollutant) and also an improved dye degradation capability under UV irradiation, compared to the free TiO$_2$ NPs, Congo Red being almost completely degraded after 70 min irradiation. It was also proved that PEGDA/TiO$_2$ hybrid film could be successfully reused several times as the photocatalyst in dyes degradation.
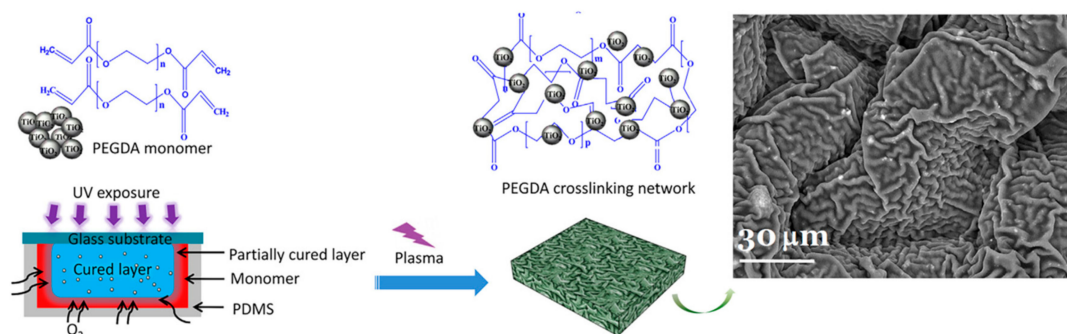
Figure 3. Schematic diagram of the preparation of PEGDA/TiO$_2$ film and SEM image of PEGDA/TiO$_2$ wrinkled composite. Reproduced by permission of Elsevier from [56].

Furthermore, TiO$_2$ was embedded in natural polymers, such as chitosan, the most abundant natural biopolymer after cellulose. TiO$_2$ NPs (1% w/v) were incorporated in two different matrices, namely chitosan (CS) and polyvinyl alcohol—chitosan blend (PVA-CS), through the precipitation method using an alkali/solvent medium [57]. The prepared materials showed superior catalytic performance in metronidazole (MNZ) removal under UV irradiation as compared to the TiO$_2$ NPs suspension, the behavior mainly attributed to the adsorption properties of the polymeric matrix. In the presence of CS-TiO$_2$ and PVA-CS-TiO$_2$ composites, MNZ at various concentrations (0.1, 1, and 10 mgL^{-1}) was almost completely degraded (more than 99%) from aqueous solutions after 120 min UV exposure, but the removal rate of PVA-CS-TiO$_2$ (4.8 × 10^{-2} min^{-1}) was higher compared to CS-TiO$_2$ (3.3 × 10^{-2} min^{-1}). PVA-CS-TiO$_2$ film proved better stability than CS-TiO$_2$ in an aqueous medium with different pH values (4 ÷ 10), it also presents very good stability under UV exposure and can be reused multiple times (15 cycles) as photocatalyst without significant loss of photocatalytic performance.

A new method used to immobilize TiO$_2$ NPs in chitosan scaffolds was 3D printing, a technique that allows the achieving of highly-ordered 3D TiO$_2$/CS grids consisting of crossing filaments with a size of about 100 μm and channels with a square cross section of 150–200 μm (Figure 4) [58].
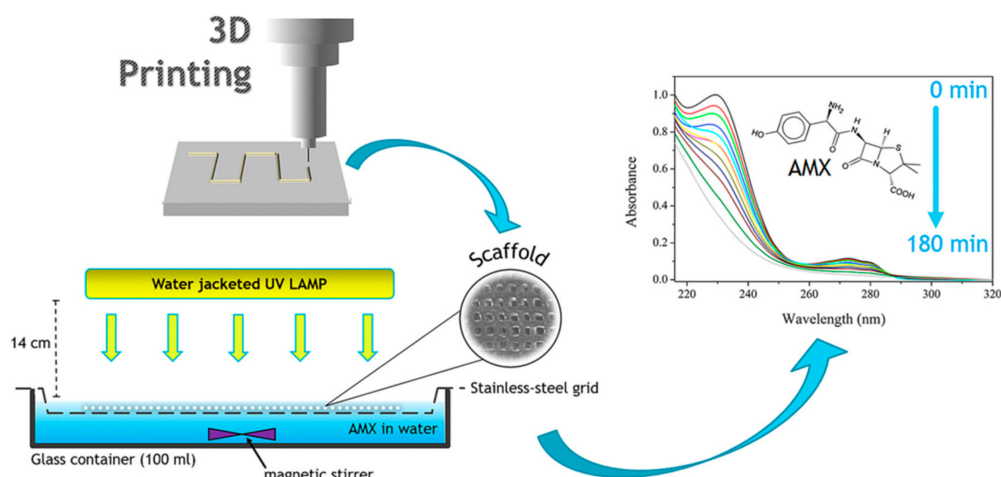
Figure 4. Schematic representation of the TiO$_2$/CS scaffolds preparation and their photocatalytic activity testing in amoxicillin photodegradation. Reproduced by permission of Elsevier from [58].

The 3D printed TiO$_2$/CS scaffolds with different thicknesses (3, 5, 15 layers) were an efficient photocatalyst for amoxicillin degradation. The time required for the complete elimination of amoxicillin is less than 3 h of UV/Vis irradiation for the three-layered one (TiO$_2$/CS$_3$, k = 0.56 × 10^{-2} min^{-1}), 3 h for the five-layered one (TiO$_2$/CS$_5$, k = 0.57 × 10^{-2} min^{-1}), meanwhile in the case of the scaffold with 15 layers (TiO$_2$/CS$_{15}$, k = 0.28 × 10^{-2} min^{-1}), after 3 h of irradiation only 50% amoxicillin was degraded. The TiO$_2$/CS$_5$ composite reusability test proved that it maintains a good photocatalytic efficiency (80%

amoxicillin was photodegraded after three cycles) compared to TiO_2/CS_3, in which case only 60% of amoxicillin was degraded after three cycles [58].

2.3. TiO₂-Conducting Polymers Hybrid Photocatalysts

Conducting polymers (e.g., polyaniline—PANI, polypyrrole—PPy, poly(acetylene)—PAc, polythiophene—PTh) with an extended π-conjugated electron system over a large number of monomer units have high charge carriers mobility expressed through high absorption coefficients that varied from visible light to near infrared [59,60], the reason for that is they can be used as photosensitizers for semiconductor materials, enhancing their photocatalytic activity under both ultraviolet and sunlight irradiation [61,62]. Since Riaz et al. published in 2015 a review on the role of conducting polymers in improving the TiO_2 photocatalytic activity [63], in this paper we will discuss only few recent articles published on this topic. PANI is often used as sensitizer for TiO_2 NPs, and as reported by Reddy et al. [64], the hybrid material was prepared by in situ oxidative polymerization of aniline in the presence of TiO_2 NPs, finally the inorganic nanoparticles being incorporated in the PANI matrix. The achieved materials were tested as photocatalysts under UV irradiation for degradation of RhB, MB, and phenol, and the obtained results are better than for the unmodified TiO_2 NPs, demonstrating thus the sensitizing effect of PANI. Moreover, it was observed that by increasing the concentration of TiO_2 in the hybrid materials, they exhibited superior catalytic activity, the best performance being observed for PANI/TiO_2 composites with 20 wt % NPs, with an efficiency of over 80% after 3 h of irradiation and rate constants as follows: k = 0.7642×10^{-2} min^{-1} for RhB, k = 0.684×10^{-2} min^{-1} for MB, and k = 0.38×10^{-2} min^{-1} for phenol.

A novel non-toxic hybrid composite containing TiO_2 NPs and PANI was developed by Zhao et al. [65]. In addition to these two constituents, $BiVO_4$ and graphene oxide (GO) were added to the material composition in order to induce photocatalytic activity under visible light. The catalytic activity of $BiVO_4$-GO-TiO_2-PANI (BVGTA) material was tested in the degradation of phenol and MB under visible light irradiation and compared with the efficiency of $BiVO_4$-GO-TiO_2 (BVGT) composite. The photocatalytic activity of the hybrid composite including the semiconductor polymer, BVGTA, was higher than that of BVGT, after 3 h of irradiation, the decomposition degree of phenol and MB being 80% (k = 0.886×10^{-2} min^{-1}) and 85% (k = 1.06×10^{-2} min^{-1}), respectively.

Another conducting polymer used as a photosensitizer is polypyrrole (PPy), the preparation of PPy-TiO_2 nanocomposite by chemical oxidative polymerization of pyrrole in the presence of different amounts (0.5, 1.0, 1.5, and 2.0 wt %) of TiO_2 NPs being reported [66]. The hybrid material displayed good catalytic activity under solar light irradiation against MB dye, after 90 min of illumination in the presence of PPy-2 wt % TiO_2 composite, 93% MB being removed. Furthermore, the reusability of the material was tested, observing that after the fourth cycle of utilization, the photocatalytic degradation of MB is reduced to 20%, outcome attributed to a morphological modification of the PPy-TiO_2 nanocomposites upon photodegradation. A recent study described the use of PPy-TiO_2 photocatalyst for the degradation of Reactive Red 45 dye (RR45), the composite being obtained by the same method as in the previous case, with a PPy:TiO_2 ratio of 1:100 [67]. The best photocatalytic activity was achieved at pH 6.6, when almost 98% RR45 (k = 1.08×10^{-2} min^{-1}) was degraded. Likewise, the PPy/TiO_2 composite was very efficient both under the UVA and solar irradiation, the higher rate constant being obtained under solar irradiation (k$_{solar}$ = 7.83×10^{-2} min^{-1}, k$_{UVA}$ = 6.28×10^{-2} min^{-1}). A disadvantage of this material is that the efficiency of the photocatalyst decreases to 80% after the second cycle of utilization (k$_{UVA}$ = 2.89×10^{-2} min^{-1}) due to the saturation of the catalyst surface and the aggregation of the catalyst particles.

A more complex approach to improve the photocatalytic performance of TiO_2 involves the creation of heterojunction between the conducting polymer and the metal oxide semiconductor [68]. An alternating donor-acceptor conjugated copolymer obtained by Pd-mediated polycondensation of diketopyrrolopyrrole (DPP) and t-butoxycarbonyl (t-Boc) modified carbazole (Car) was coupled with TiO_2 NPs [69]. In order to form a heterojunction interface, the achieved material was thermally treated

to cleave the pendant t-Boc groups from the carbazole units, thus creating free amino groups (-NH-) which strongly bind to the surface of TiO_2 through dipole–dipole interactions (Figure 5).
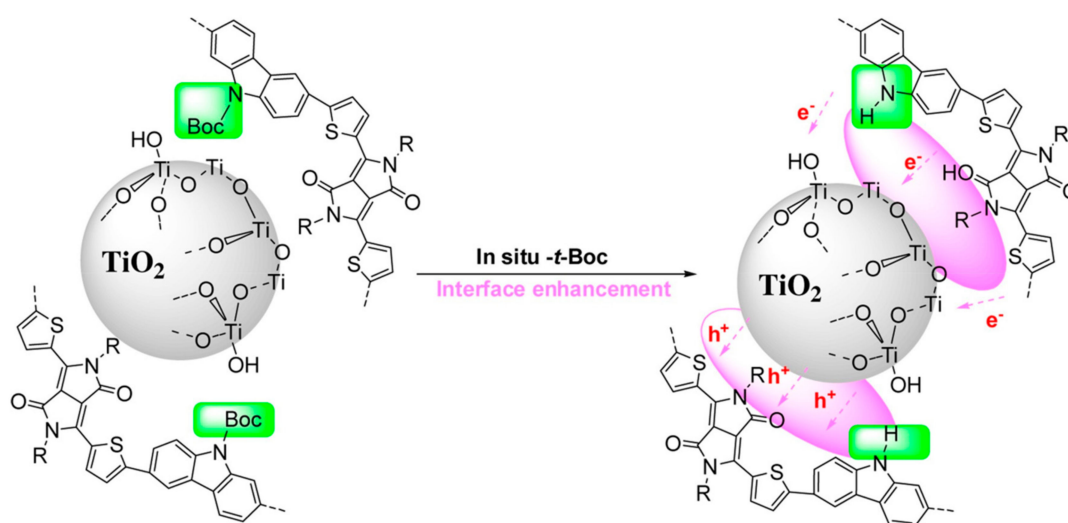
Figure 5. The proposed mechanism for the formation of heterojunction interface interaction to enhance photocatalytic efficiency. Reproduced by permission of Elsevier from [69].

The resulting DPP-Car/TiO_2 hybrid composites presented light absorption within the range of 300–1000 nm, unlike pure TiO_2 (P25) which does not have effective visible light absorption (>400 nm). DPP-Car/TiO_2 hybrid materials were tested as photocatalysts for MO dye degradation under visible light, the decomposition degree was 94% after 8 h of irradiation and the rate constant was k = 0.563×10^{-2} min^{-1}. The kinetic constant of MO degradation in the presence of the thermally treated sample (DPP-Car/TiO_2) is about 3.6 times higher than that obtained in the presence of the catalyst containing t-Boc units (DPP-Car-Boc/TiO_2: k = 0.155×10^{-2} min^{-1}). The recycling experiments performed to test the durability and stability of the composites showed that the photocatalytic efficiency of MO degradation slightly decrease in the second and third cycles compared with that registered in the first cycle.

Starting from poly (3-hexylthiophene), Che et al. [70] prepared by a phase-separated film shattering process, conjugated polymer nanoparticles (P3HT) with positive surface charges by adding a cationic amphiphile and a phospholipid. Subsequently, the P3HT NPs were hybridized with negatively charged TiO_2 NPs by their adsorption on the positively charged surfaces through electrostatic attraction, the P3HT:TiO_2 molar ratios used were 1:0.2, 1:0.6, and 1:1. TEM and SEM images revealed that the surface of P3HT NPs was covered by TiO_2 NPs, so the resulting hybrid material is a core-shell system with a conjugated polymer core and a shell constituted of photocatalyst nanoparticles. The photocatalytic activity of hybrid nanoparticle systems was evaluated in MB degradation under white light and visible light irradiation, the best efficiency being obtained under white light irradiation for the hybrid material with higher P3HT content, namely P3HT/TiO_2 with molar ratio 1:0.2 (after 210 min of white light irradiation, 93.4% of MB was degraded, k = 0.992×10^{-2} min^{-1}).

Poly-*o*-phenylenediamine (PoPD), a typical conducting polymer, has been used to synthesize PoPD/TiO_2 nanocomposites via in situ oxidative polymerization of *o*-phenylenediamine in the presence of TiO_2 NPs, using different initial molar ratios of oPD/TiO_2 (from 1/6 to 4/1) [71]. To investigate the photocatalytic activity of the composites, MB degradation under visible light was selected as a model reaction, establishing that the optimum molar ratio for preparing materials with high photocatalytic efficiency (k = 0.33×10^{-2} min^{-1}) and stability (recycled five times, 15 h of operation) is 1/4.

3. ZnO Nanoparticles

ZnO nanoparticles with different morphologies and properties have received a great deal of attention for photocatalytic applications, both in the field of environmental pollution and energy conversion [72]. Originally proposed as an alternative photocatalyst to TiO_2, ZnO is a n-type semiconductor oxide possessing wide band gap energy (3.37 eV), high photoactivity, non-toxicity, and environmental stability [73,74], which has developed unique and remarkable photocatalytic capacity over time, since it is able to absorb a large part of the solar spectrum with relevant performance in the photodegradation of toxic and nonbiodegradable organic contaminants, including organic dyes, phenols or other environmental pollutants [75–77], etc.

ZnO benefits from great advantages compared to other semiconducting metal oxides and represent an environmentally friendly material. Its use in everyday application is done without any risks to human and living organism health. Along with excellent electrical, mechanical, and optical properties [78], ZnO is a cheaper material compared to TiO_2 (the production cost up to 75%, according to Liang et al. [79]), whereby it is much appreciated and explored for large scale operations [80,81]. Unfortunately, the major drawback of ZnO nanoparticles is associated with their narrow spectral response, when the light absorption is almost limited to UV domain. Consequently, considerable efforts were done to overcome this inconvenience along with characteristic high probability for the recombination of photogenerated charge carriers. Innovative approaches demonstrated that by coupling the ZnO with various narrow band-gap materials (metallic and nonmetallic ions [82–84] noble metals and oxides [85–88] or polymer-based materials [89,90] etc.), it was possible to modulate the band-gap energy and shift the absorption wavelength to the visible region. The photogenerated electron-hole pair recombining is also suppressed, while the photocatalytic activity of ZnO is consequently enhanced.

Basically, the efficiency of the photocatalysis process depends on the morphology, dimension, or shape of the investigated semiconductor oxides. Therefore, an excellent control and understanding of synthesis conditions are critical for the development of novel and high-performance photocatalysts characterized by efficient separation of charge carriers, increased surface-to-volume ratio, and light absorption capacity with superior stability/reusability features. Therefore, the incorporation and immobilization of ZnO nanostructured materials into polymers could represent a strategic approach to benefit from advantages of each component, in order to obtain improved photocatalytic systems. The significant features targeted are the flexibility of the final architecture, the control over agglomeration/aggregation and the elimination of the post-recovery steps specific to unbounded catalyst particles after the photocatalytic process.

Several reports on nanostructured ZnO are correlated to their practical and safe incorporation into various macromolecular matrices, such as poly (N-isopropylacrylamide) [91], polyesters [88], hybrid polymers [92,93], polyethylene glycol [94], etc., but are not necessarily associated with the photocatalysis process. From the abundant reports referring to the augment of the photocatalytic efficiency of ZnO nanomaterials toward visible light, polyaniline (PANI) has attracted much attention and is considered one of the great potential materials for improving the photocatalytic and electrochemical performance of ZnO. Another interesting aspect is that almost all reports select methylene blue (MB) as a model pollutant to evaluate the photocatalytic activities under UV/visible light irradiation, at room temperature. Qin et al. [95] reported superior photocatalytic activity of PANI-ZnO nanoparticles (reaction rate constant k = 1.944×10^{-2} min^{-1}) over a large concentration of MB. Polyaniline-zinc oxide (PANI-ZnO) nanocomposites were prepared by in situ chemical polymerization process, and thus, one of the pre-request conditions of an efficient photocatalyst is fulfilled. Moreover, the PANI-ZnO hybrids prepared in this study were used to decorate glassy carbon electrode (GCE) and the final system PANI-ZnO/GCE was investigated for its potential as a microbiological fuel cell anode, too.

In another report, Ameen et al. [96] prepared PANI/ZnO nanocomposites, the outcomes of the photocatalytic activity indicating a substantial degradation of MB dye (approximately 76%) on the surface of PANI/ZnO catalyst under visible light illumination. The PANI/ZnO system showed a photocatalytic activity three times higher in MB dye degradation as compared to the pure PANI,

behavior attributed to the high charge separation of electron and hole pairs in the excited states of coupled PANI-ZnO nanocomposites.

For the same purpose, Eskizeybek et al. [97] synthesized PANI/ZnO nanocomposites via chemical oxidative polymerization of aniline and investigated the degradation of two dyes in solutions (MB and malachite green (MG) dyes in aqueous medium) under natural sunlight and UV light irradiation. Final results indicated that a small amount of PANI/ZnO nanocomposite photocatalyst (0.4 g/L) degrades both of the dye solutions (MB or MG) with 99% efficiency after 5 h of irradiation under natural sunlight. Instead, Saravanan et al. [98] obtained PANI/ZnO nanocomposites with superior activity due to the increase of crystallinity and intermolecular interactions between the conducting polymer and ZnO NPs, and further investigated the rapid degradation of MB ($k = 2.575 \times 10^{-2}$ min^{-1}) as compared to MO dye ($k = 2.325 \times 10^{-2}$ min^{-1}), probably due to their simpler structure.

Metronidazole (MNZ) is a synthetic antibacterial agent, known for its non-biodegradability and high solubility in water, therefore its removal from the wastewaters before being discharged into the environment has gained important attention. Very recently, Asgari et al. [99] investigated the photocatalytic potential of ZnO/PANI nanocomposites for the degradation of MNZ under UV and visible light irradiation. They established that the degradation rate of MNZ by the ZnO/PANI nanocomposite ($k = 2.53 \times 10^{-2}$ min^{-1}) was almost 63 times higher than for the pure ZnO photocatalyst ($k = 0.04 \times 10^{-2}$ min^{-1}) and proposed a diagram for the photocatalytic mechanism of this system (Figure 6).
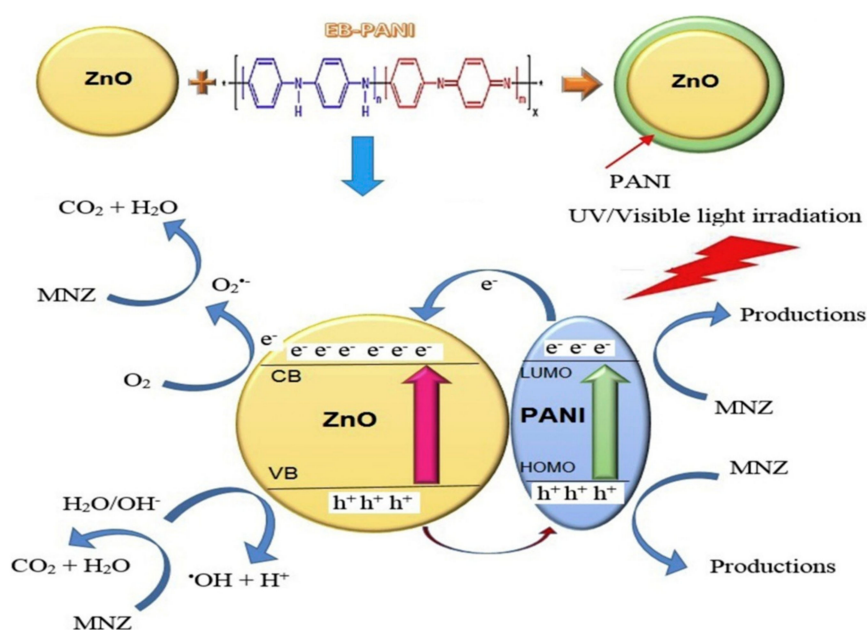
Figure 6. Diagram of the photocatalysis mechanism in ZnO/PANI nanocomposite under UV and visible light radiation. Reproduced by permission of Elsevier from [99].

The role of hydroxyl radicals (•OH) and superoxide anion radical (•O$_2$$^-$) in MNZ degradation was highlighted. The photocatalytic performance under UV and visible irradiation was associated with the improvement of the visible light absorption and the reduction of charge carrier recombination.

Composite photocatalysts consisting of polypyrrole (PPy) and ZnO particles were prepared by the polymerization of pyrrole in the presence of wurtzite type ZnO nanoparticles, the ratios of PPy to ZnO in the final composites being 5:1 and 25:1 [100]. The photocatalytic activity of PPy-ZnO composites was established by studying the degradation of diclofenac (DCF) drug under simulated solar light irradiation at ambient conditions. The performed investigations pointed out that the photocatalytic rate constant of PPy-ZnO 25:1 ($k = 0.986$ min^{-1}) was higher than for the PPy:ZnO 5:1 composite and nearly two times higher than that of ZnO. This improvement in the photodegradation efficiency of

PPy-ZnO composites has been attributed to a sensitizing effect of PPy, however, a high PPy:ZnO ratio can inhibit the active sites on the PPy surface, causing defects that can act as recombination centers between e^-/h^+ pairs, reducing thus the photocatalytic activity as in the case of PPy:ZnO 5:1 composite. The reuse studies performed on PPy-ZnO 25:1 composite showed that there was no significant decrease in photocatalytic activity after three subsequent degradation cycles.

In the attempt to find the most effective solutions to enhance the photocatalytic efficiency of ZnO nanoparticles immobilized in polymeric substrates, Ding et al. [101] prepared hierarchical polyimide/ZnO flexible nanofiber membranes by a combination of electrospinning and direct ion-exchange process. They firstly prepared poly (amic acid) nanofibers by electrospinning and subsequently immersed the resulting membranes into $ZnCl_2$ solutions. By the thermal treatment of the nanofibers, the imidization of poly (amic acid) to polyimide and the formation of ZnO nanoparticle took place simultaneously. By simply changing the concentration of $ZnCl_2$ solution, ZnO nanoparticles can be obtained on the electrospun nanofibers as nanoplatelets or nanorods, thus offering the possibility to obtain wide range nanomaterials with tunable photocatalytic activity. The photocatalytic properties of the composite polyimide/ZnO membranes were evaluated in MB degradation as a model organic pollutant. The degradation rate constants of 0.2 M PI/ZnO ($k = 1.66 \times 10^{-2}$ min^{-1}), 0.5 M PI/ZnO (2.83×10^{-2} min^{-1}), 1 M PI/ZnO (2.16×10^{-2} min^{-1}), and 2 M PI/ZnO (1.0×10^{-2} min^{-1}) composite membranes showed that the higher photocatalytic efficiency was achieved for 0.5 M PI/ZnO nanofiber membrane.

Poly (methyl methacrylate) (PMMA) represents another frequently used polymeric matrix employed in many applications as a result of its specific properties (low-cost, transparency to visible light, superior mechanical properties, chemical stability, etc.). Different research groups tested the photocatalytic performance of ZnO/PMMA composites in wastewater treatment. More precisely, Di Mauro et al. [102] coated PMMA powders with a thin layer of ZnO (80 nm thick) by atomic layer deposition (ALD) method, at low temperature (80 °C). The photocatalytic efficiency was tested on the degradation of MB dye and toxic phenol in aqueous solution, under UV light irradiation. The synthesized ZnO/PMMA powders induced a degradation of about 60% of MB after 4 h of irradiation ($k = 0.41 \times 10^{-2}$ min^{-1}), the ZnO/PMMA composite film was able to degrade almost 40% of the dye after 240 min, with a photodegradation rate $k = 0.26 \times 10^{-2}$ min^{-1}, while ZnO flat film degraded nearly 30% of MB after 240 min with a photodegradation rate $k = 0.17 \times 10^{-2}$ min^{-1}. Moreover, it was demonstrated that the resulting ZnO/PMMA nanocomposite was stable and reusable for seven successive MB discoloration runs.

A comparative study involving the PMMA matrix was done by Rani and Shanker [103], which reported the green synthesis and photocatalytic activity measurements of different metal oxides-poly(methyl methacrylate) (MO-PMMA) nanocomposite, including ZnO nanoparticles. Therefore, Fe_3O_4-PMMA, ZnO-PMMA, CuO-PMMA, and Ni_2O_3-PMMA were prepared and tested as a photocatalyst for methylene blue degradation into non-toxic by-products (Figure 7). The best results were obtained for ZnO-PMMA (99%) followed by Ni_2O_3-PMMA (98%), CuO-PMMA (93%), and Fe_3O_4-PMMA (90%), the effect probably due to the high surface area (85.32 m^2 g^{-1}) and zeta potential (-22.5 eV) of the composite. Moreover, the reusability test of the nanocomposite for up to 10 times proceeds without significant change in the photocatalytic activity or in the structure of the materials.
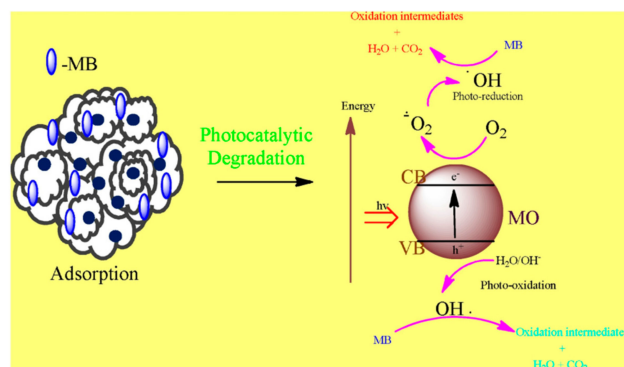
Figure 7. Schematic illustration of the adsorption and photocatalytic degradation of MB over (MO-PMMA) nanocomposite photocatalysts. Reproduced by permission of Elsevier from [103].

Cellulose, an abundant organic material involved in various applications, such as drug delivery, composite materials, packaging, textile industries, etc. has also been considered as a supporting material for photocatalysts, including ZnO nanoparticles. As a result, Lefatshe et al. [104] prepared zinc oxide (ZnO) nanostructures in the cellulose host polymer through in situ solution casting method, in order to improve the antibacterial and photocatalytic efficiency of ZnO NPs. They have studied the photocatalytic activity of zinc oxide/cellulose nanocomposite in MB photodegradation under UV irradiation in comparison with the pure ZnO nanostructures, observing that the efficiency of ZnO dispersed in nanocellulose matrix ($k = 0.19 \times 10^{-2}$ min^{-1}) was better than for the pure ZnO nanostructures ($k = 0.17 \times 10^{-2}$ min^{-1}). This fact was attributed to the high surface area supplied by cellulose, which increases the number of active sites per square meter and generates an enhanced reactivity of the composite [105].

In a further study, Rajeswari et al. [106] described the preparation of cellulose acetate-polystyrene (CA-PS) membrane bearing ZnO nanoparticles, material characterized by an enhanced photocatalytic efficiency and high thermal stability. The effectiveness of the material in the organic pollutants degradation (Congo red and Reactive yellow-105) was tested under solar irradiation, according to the schematic set up illustrated in Figure 8. The complete degradation of the pollutants was reached after 40 min of irradiation at neutral pH, when the degradation yield of CR and RY-105 was 95% and 98%, respectively. The reusability study indicated that no significant changes were observed until the fourth cycle, suggesting a good stability and reusability of the CA-PS-ZnO membrane under sunlight irradiation.

Figure 8. Schematic representation of the photocatalytic degradation of organic dyes over CA-PS-ZnO membrane. Reproduced by permission of Elsevier from [106].

The design of new polymer nanocomposites combining 2-hydroxyethyl methacrylate monomer (HEMA), graphene oxide (GO) filler, and ZnO nanolayers in a unique multifunctional material was reported by Ussia et al. [107]. ZnO nanoparticles were immobilized on the polymeric support through stable covalent linkages, while GO filler was added during the synthetic procedure to improve the thermal and mechanical stability of the material, resulting in the formation of a freestanding photocatalytic material, easily and safely removable from the polluted environments. The system showed a significant adsorption affinity for methylene blue dye, so at equilibrium, the amount of adsorbed MB was of 0.73, 0.97, 0.82, and 0.94 mg/g of materials, for pHEMA, pHEMA-GO, ZnO/pHEMA, and ZnO/pHEMA-GO, respectively. After the adsorption process, the nanocomposites were subjected to UV light irradiation, when MB is photocatalytically degraded, leading to the initial regenerated composite. The performed studies have shown that pHEMA and pHEMA-GO samples lose their adsorption capability after several cycles, while the samples containing ZnO NPs are able to preserve their adsorption and photocatalytic performance thanks to the regeneration via UV light irradiation.

In a comparative study, Ghanem et al. [108], after the prior preparation of TiO_2 nanowires modified with hyperbranched polyester (HPES) [109], compared the system from the photocatalytic activity point of view, with similar ZnO nanorods-based hybrid composites. The authors used both in situ polycondensation reaction (I-HPES/ZnO) and ex situ mixing technique (E-HPES/ZnO) to obtain the final nanocomposites. Photocatalytic activity testing revealed a good performance of the prepared ZnO-based hybrids after repeated photocatalytic degradation cycles, evidencing the reactivity improvement for ZnO nanorods after modification with HPES. The best photocatalytic activity was observed for the E-HPES/ZnO composite behavior due to the higher surface area, crystallite size, and larger band gap of this nanocomposite. In addition, antibacterial investigations demonstrated enhanced nanotoxicity for both Gram-positive and Gram-negative bacteria, the fact that will bring additional applicative value for the final nanocomposites.

Photocatalysis represents a complex process mainly governed by the band-gap energy of the components and the hydroxyl radicals generated in the system. Unfortunately, the major drawback of ZnO is associated with its light absorption, almost limited to UV domain. Therefore, considerable efforts were done to overcome this inconvenience and one of the strategies was the coupling/combination of ZnO with a variety of narrow band-gap materials (especially metallic and nonmetallic ions), known as the doping process. This practice aims to adjust the morphology of ZnO for photocatalytic applications, by tuning the band-gap energy and, consequently, shifting the absorption wavelength toward a visible region. In addition, doping can trigger the production of OH• radicals and can also improve the degradation efficiency of organic pollutants. Among the commonly used dopants, transition metals (Fe, Co, Ni, Cu, etc.) and noble metals (Au, Ag, Pd, Pt, etc.) stand out, certainly.

In this context, the development of doped ZnO nanoparticles included in different macromolecular architectures for applications in the removal of organic aqueous pollutants through heterogeneous photocatalytic approach represents an expanding area in the recent literature. Therefore, Campagnolo et al. [110] presented the preparation of hybrid photocatalysts on a porous solid polymeric system for the heterogeneous photocatalytic degradation of organic pollutants. More specifically, gold/zinc oxide (Au/ZnO)-based porous nanocomposites were in situ fabricated by a two-step approach: First, branched ZnO nanostructures were fixed on poly (methyl methacrylate) (PMMA) upon the thermal conversion of zinc acetate-loaded PMMA electrospun mats, while doping with Au NPs was done directly on the surface of ZnO through an adsorption dipping process followed by thermal treatment. The authors also investigated the effect of the various concentrations of Au NPs formed on the surface of the ZnO/PMMA fibers, establishing an effective metal-semiconductor interfacial interaction for a concentration of 1 wt % Au NPs. As a result, a significant improvement in the photocatalytic performance of ZnO/PMMA electrospun nanocomposites bearing Au NPs in the degradation of MB (k = 2.33×10^{-3} min^{-1}) and bisphenol A (BPA) (k = 1.12×10^{-3} min^{-1}) was observed in comparison to pure the ZnO/PMMA nanocomposites (k = 1.44×10^{-3} min^{-1} for MB

and k = 0.69×10^{-3} min^{-1} for BPA). Unfortunately, the photocatalytic degradation activity of the Au/ZnO-based PMMA hybrid systems was tested only under UV light irradiation.

In a different report, enhancement of visible light photocatalytic activity and plasmonic electron-hole separation efficiency were obtained by decorating a ZnO nanolayer coated onto electrospun polyacrylonitrile (PAN) nanofibers with Pd nanocubes (with sizes varying between 7, 13, and 22 nm), as illustrated in Figure 9 [111]. The photocatalytic activity of the obtained nanofibers (Pd@ZnO@PAN-NF versus ZnO@PAN-NF) was analyzed by the photoinduced degradation of MB dye under visible irradiation, in aqueous medium, when the energy transfer between Pd nanocubes and ZnO nanolayer was clearly demonstrated. Moreover, the electron-hole recombination rate of the photogenerated electrons and holes was reduced by the electron trapping via Pd nanocubes. The degradation kinetics of the photoprocesses showed that the sample decorated with 7 nm Pd nanocubes had the highest photocatalytic activity, while the ZnO@PAN-NF sample showed no decomposition of MB dye under the given conditions.
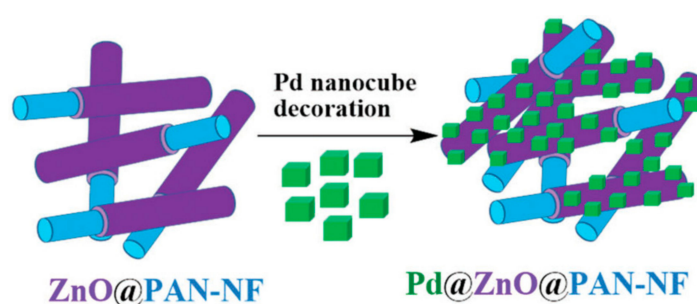
Figure 9. Representation of Pd nanocube surface decoration on ZnO@PAN nanofibers. Reproduced by permission of The Royal Society of Chemistry from [111].

New hybrid composites including ZnO and Ag/ZnO NPs have been successfully prepared in our group by Podasca et al. [88]. The hybrid films were achieved by photopolymerization of some urethane acrylic monomers simultaneously with the in situ photogeneration of Ag nanoparticles under UV light irradiation, ZnO NPs being included in the monomer mixture as preformed particles before photopolymerization. The final composite films containing ZnO, Ag, and Ag/ZnO NPs in different ratios were employed as catalysts for photocatalytic decomposition of MB dye in ethanol or water solvents. The degradation experiments were realized under both UV and visible irradiation, but in different solvents. Under UV irradiation and ethanol solvent, as expected, the ZnO-Ag/polymer film had an improved degradation rate of MB (k = 1.37×10^{-2} s^{-1}) compared to ZnO/polymer film (k = 2.7×10^{-2} s^{-1}). In this solvent, the leakage of Ag NPs from the polymeric film was also observed, so the visible light experiments were performed in ethanol and also in aqueous solution. Only films containing ZnO and Ag NPs exhibited catalytic activity under visible light. The decomposition rate of MB was lower by an order of magnitude in aqueous solution (k = 2.1×10^{-2} min^{-1}) than in ethanol (k = 1.1×10^{-1} min^{-1}), however, no leakage of nanoparticles was observed, thus proving that the catalyst can be reused. As a continuation of this study, the same group [112] recently reported the preparation of novel polymer nanocomposites containing Ag/ZnO NPs and polypyrrole, in which silver nanoparticles were also in situ photogenerated during the curing process. The obtained films were investigated and successfully used as a visible light photocatalyst for the degradation of rhodamine B dye in aqueous solution. It was observed that RhB degradation occurred with rate constant k = 2.96×10^{-2} min^{-1} in the presence of ZnO-Ag-PPyr film and with a rate constant k = 2.99×10^{-2} min^{-1} in the case of ZnO NPs film.

In an interesting report, Sarro et al. [113] used a rare earth ion doping to induce photocatalytic efficiency improvement to ZnO nanoparticles. Thus, they tested for the first time, a new hybrid material which combines Ce/ZnO photocatalyst with polymer nanofibers (poly(styrene-*co*-maleic anhydride); SMA) and soybean peroxidase (SBP) in order to obtain a stable and efficient system useful for the

degradation of organic pollutants in wastewater treatment. The ability of the achieved materials to degrade six emerging wastewater pollutants, namely diclofenac, naproxen, iopamidol, imidacloprid, bisphenol A, and 2,4-dichlorophenol was tested as single contaminants in MilliQ water or as pollutants mixture in MilliQ water and wastewater. It was found that Ce-doped ZnO photocatalyst, included in SMA nanofiber and in the presence of SBP enzyme exhibited higher photocatalytic efficiency in degradation of the targeted pollutants in the effluent wastewater (the kinetic constants for different contaminants are in the range $0.35–1.3 \times 10^{-3}$ min^{-1}). The practical importance of the polymer supporting the other components and the successful combination between Ce-doped ZnO with SBP with the aim to enhance the oxidation capability of the system towards pollutant with different chemicals properties was also highlighted.

4. CeO$_2$ Nanoparticles

Another interesting metal oxide displaying a huge potential to provide sunlight active photocatalysts is nanoceria (cerium oxide nanoparticles CeO$_2$), one of the most reactive rare earth oxides with advantageous properties such as wide band gap (E$_g$ = 3.19 eV) and high dielectric constant (ε = 24.5) [114]. These properties have generated important interest and nanoceria have found numerous applications in the field of solar cells, oxygen sensors, electrolytes in solid oxide fuel cells, dye removal, ultraviolet absorbers, or catalysis [115]. The reversible shift of the oxidation state between Ce^{3+} and Ce^{4+} determine the formation of oxygen vacancies that are directly responsible for the catalytic ability of CeO$_2$ nanoparticles, an enhanced level of Ce^{4+} ions contributing to superior photocatalytic activity of nanoceria [116]. Furthermore, CeO$_2$ nanoparticles showed interesting properties (strong oxidizing capacity, long-term stability, nontoxicity, low cost, high electron transfer capability) that recommend them as efficient photocatalysts for environmental applications [117]. However, as in the case of most inorganic nanoparticles, nanoceria exhibits a strong tendency to agglomerate/aggregate which leads to a significant decrease in the catalytic activity by reducing their surface area and additionally, their recovery and reuse tends to be quite difficult [118]. A convenient method to avoid these problems consists in the immobilization of CeO$_2$ nanoparticles on polymeric supports resulting in hybrid materials with improved performances (optical, electrical, mechanical) compared to the starting materials due to the synergistic effect manifested by each partner on the final characteristics of the polymer nanocomposites. Although the literature data reported up to now of numerous studies regarding the synthesis of polymer/ceria nanoparticles hybrid composites [119–121], few studies were focused on the preparation of CeO$_2$/polymer hybrid materials with applications in the photocatalytic degradation of organic pollutants, a main source of water pollution.

Thus, Fischer et al. [122] proposed the preparation of cerium oxide/polystyrene nanoparticles functionalized at the surface with phosphonate and phosphate groups that acts as nucleation centers and stabilizers for the controlled in situ crystallization of cerium oxide nanocrystals. The photocatalytic activity of CeO$_2$/polymer hybrid particles was tested in the photodegradation of rhodamine B irradiated with UV light at constant temperature. The study pointed out that the photooxidative degradation of RhB occurred with a higher rate in the presence of CeO$_2$/polystyrene nanoparticles ($k = 2.86 \times 10^{-2}$ min^{-1} and $k = 4.36 \times 10^{-2}$ min^{-1} for the CeO$_2$/phosphonate and CeO$_2$/phosphate hybrid particles) than without catalyst or in the presence of commercial cerium (IV) oxide powders ($k = 1.59 \times 10^{-3}$ min^{-1}), proving the efficiency of the hybrid system on the rhodamine B photodegradation.

In a more recent study, the preparation of poly (vinylidene fluoride-*co*-hexafluoropropylene) (PVDF-HFP)/cerium oxide (CeO$_2$) nanocomposite fibrous membranes was reported by Morselli et al. [123]. The fibrous membranes were fabricated by a facile method, combining the electrospinning and the in situ synthesis of ceria nanoparticles directly in electrospun polymeric fibers by the thermally activated conversion of the precursor salt in CeO$_2$ nanoparticles. Moreover, to improve the photocatalytic degradation activity of the fibers, gold nanoparticles were synthesized by thermal treatment in situ in tandem with the ceria ones directly in the polymeric fibers (PVDF/CeO$_2$/Au_in)

or ex situ by post thermal treatment (PVDF/CeO$_2$/Au_ex), resulting in valuable systems with enhanced properties for water purification or bioapplications triggered by visible light irradiation. The photocatalytic activity was tested on MB degradation under visible light irradiation, observing that PVDF-HFP/CeO$_2$ membrane display the same photodegradation efficiency as the neat PVDF-HFP membranes (k = 0.8×10^{-3} min^{-1}), indicating that ceria nanoparticles does not exhibit any significant photocatalytic activity under visible light irradiation, while the inclusion of Au NPs determine an important improvement of the photocatalytic activity for the PVDF/CeO2/Au_ex fibrous membrane (k = 1.4×10^{-3} min^{-1}). These results are attributed to a decrease of band gap values from 3.26 to 3.18 or even to 2.97 eV for the gold-containing samples, the fact that allows the activation of photodegradation process by visible light.

In another recent study, the facile two-step fabrication of a ternary nanocomposite particle composed of polystyrene (PS) microsphere, reduced graphene oxide (RGO), and CeO$_2$ NPs was reported by Ni et al. [117]. The photocatalytic activity of the ternary nanocomposite particles was demonstrated by the investigation of methylene blue photodegradation under visible light irradiation. It was observed that the photocatalytic activity of CeO$_2$ NPs is highly enhanced by the hybridization with the RGO due to a positive synergistic effect between RGO and ceria nanoparticles (k = 1.5×10^{-2} min^{-1}). Moreover, these nanocomposite particles could be easily recovered by centrifugation and could be reutilized for several catalytic cycles, thus indicating PS/RGO@CeO$_2$ nanocomposite particles as a promising recyclable photocatalyst for methylene blue degradation.

5. Metal Nanoparticles (Au, Ag, Pd)

Metal nanoparticle photocatalysts are currently intensively investigated due to their unique quantum effect translated into strong absorption of visible and ultraviolet light. They have been acknowledged as a new class of materials very efficient in transforming renewable solar energy to chemical energy due to their strong interaction with resonant incident light through the localized surface plasmon resonance (LSPR) effect [124]. Their activation mechanism consists in the accumulation of the irradiation energy by the conducting electrons of the metal nanoparticles that lead to the formation of high energy electrons on the surface of the nanoparticles, electrons that further will activate the target molecules on the surface of the particles and will trigger the chemical reactions. However, as in the case of metal oxide nanoparticles, a great challenge is to achieve catalytic systems active under visible light irradiation, easily separable and reusable that can be applied in organic pollutants degradation or in organic chemical synthesis. The catalytic properties of noble metal nanoparticles depend to a large extent on the size, geometry, and distribution of the nanoparticles, as well as on the interactions between them and the support materials. Therefore, as potential supports for metal nanoparticles immobilization various materials can be used, such as carbon-containing materials, polymers, mesoporous materials, insulating solids, MOF materials, etc. In the present work, we will refer only to polymeric systems embedding metal nanoparticles employed in photocatalytic processes.

In one of the first attempts, Saeed et al. [125] prepared by the electrospinning technique polyacrylonitrile nanofibers (PAN) modified with amidoxime units. Further, the nanofibers were used to chelate Ag$^+$ ions that were reduced by hydrazine into elemental silver nanoparticles. The photocatalytic activity of Ag/OM-PAN nanofibers was evaluated by monitoring the degradation of methyl orange dye in aqueous solutions under UV irradiation as a function of time, observing that Ag/OM-PAN significantly degraded the dye in comparison with the unmodified PAN nanofibers with no effect on the dye photodegradation. The photocatalytic activity of Ag/OM-PAN nanofibers is induced by the presence of silver nanoparticles which, by the localized effect of surface plasmon resonance (LSPR), are capable to degrade MO in an aqueous solution. Thus, upon irradiation, the conduction electrons of silver nanoparticles are excited as high energy electrons on the surface of the nanoparticles [19]. Then, it is supposed that the excited electrons easily react and activate dye molecules leading to their subsequent decomposition.

Jana et al. have designed raspberry type organic-inorganic hybrid nanostructures of poly-3-hexylthiophene (P3HT)—Au nanoparticle (NP) composite prepared by a simple solution-based synthetic technique [126]. The photocatalytic activity was carried out under visible light irradiation by following the photodegradation efficiency of MB in the presence of P3HT and P3HT/Au NPs polymer nanoparticles. It was observed that the presence of Au nanoparticles on the P3HT surface determined an increase of the degradation efficiency form 55% for P3HT to 90.6% for P3HT/Au NPs after 180 min of visible irradiation, confirming thus the contribution of gold nanoparticles on the overall photodegradation process investigated in this case.

In another study, Ghosh et al. prepared hybrid nanostructures based on poly (3,4-ethylenedioxythiophene) (PEDOT) nanofibers and gold nanoparticles (Au NPs) through a one pot interfacial polymerization method [127], obtaining conductive polymer nanofibers with synergistically integrated plasmonic Au NPs (~6 nm). The photocatalytic activity in organic pollutant degradation of Au/PEDOT and PEDOT nanofibers was evaluated by using methyl orange and rhodamine B dyes under both UV and visible light irradiation, observing that Au/PEDOT nanofibers demonstrate superior photocatalytic activity ($k = 7.3 \times 10^{-2}$ min^{-1} and $k = 5.6 \times 10^{-2}$ min^{-1}, for MO and RhB, respectively) as the PEDOT polymer ($k = 2.9 \times 10^{-2}$ min^{-1} for MO and $k = 1.9 \times 10^{-2}$ min^{-1} for RhB), while compared to traditional Au/TiO$_2$ catalyst, the kinetic constant is over 46 times higher ($k = 0.16 \times 10^{-2}$ min^{-1} for MO and $k = 0.13 \times 10^{-2}$ min^{-1} for RhB). Moreover, the recovery and recyclability of the Au/PEDOT photocatalyst was tested, observing that after five cycles under visible irradiation, the photocatalyst retained up to 95%–98% of its original activity, recommending thus Au/PEDOT as a stable and efficient photocatalyst for the degradation of organic pollutants.

A different approach to achieve photocatalytic materials consists in the preparation of environmental friendly, low cost films by blending natural rubber latex with polyvinylpyrrolidone (PVP) of different molecular weights and impregnation of the resulting films with silver ions (Ag$^+$) which by treatments at low temperature are converted to silver particles (Ag^0), research reported by Abu Bakar et al. [128]. They have tested the photodegradation of MO under sunlight using natural rubber-blend-PVP/silver (NR-b-PVP/Ag) films, observing that MO photodegradation is influenced by the molecular weight of PVP, MO concentration, and Ag content in the samples. The highest rate constant value k, obtained for the MO degradation by using the NR-b-PVP/Ag film with PVP M$_w$ of 360 was $k = 2.61 \times 10^{-2}$ min^{-1}. Additionally, the authors studied the photodegradation of bromocresol green, methylene blue, and p-nitrophenol in the presence of NR-b-PVP/Ag film, in order to prove the versatility of the reported materials to degrade various types of organic pollutants.

Recently, Hareesh et al. prepared silver/polycarbonate (Ag/PC) and gold/polycarbonate (Au/PC) samples by the Synchrotron X-ray radiation assisted method [129]. They studied the photocatalytic degradation of MB dye in the presence of Ag/PC and Au/PC samples under UV irradiation, observing that MB is photodegraded at higher rates in the presence of Ag/PC and Au/PC samples comparative to the individual nanoparticles. This result can be attributed to the agglomeration of unbounded Ag or Au NPs, which decreases the surface-to-volume ratio and consequently the speed of photocatalytic degradation.

Polymer nanocomposite films prepared by in situ photogeneration of gold nanoparticles in tandem with the photopolymerization process of methacrylated glycomonomers with D-glucofuranose or D-mannitol structural units that were reported by our group [53]. The nanocomposites were synthesized by a simple, efficient, cheap, and eco-friendly method that allow the achieving of flexible free-standing films active in the photocatalytic degradation of MB and MO dyes in aqueous phase under visible light irradiation at ambient temperature. The photodegradation of MB proceeds for the most active sample with a rate constant of 4.7×10^{-2} min^{-1}, while in the case of MO dye, the calculated rate constant was 3.18×10^{-2} min^{-1}, values comparable to other photocatalytic systems. Further, the reusability of the hybrid polymeric films containing Au NPs was tested on MB photodegradation, observing that the catalytic activity is slightly diminished as for the first catalytic cycle, the calculated rate constant being of 3.49×10^{-2} min^{-1}, this fact is attributable to a reduction of the adsorption capacity of the dye by the hybrid material.

A step forward in the design of photocatalytic systems was made by the preparation of bimetallic nanocomposite films embedding Au–Ag nanoparticles photogenerated simultaneously with the photopolymerization process [130]. The evaluation of the photocatalytic degradation of 4-nitroaniline under visible irradiation in aqueous solution showed an improvement of the catalytic activity for the hybrid material containing Au–Ag NPs comparatively with the samples including only Au or Ag nanoparticles (synthesized for comparative purposes) behavior that can be accounted to the synergistic effect between Ag and Au nanoparticles with superior catalytic efficiency relative to their monometallic counterparts. Furthermore, the inclusion of a phenylboronic acid derivative in the organic matrix triggered the photoreduction of 4-nitroaniline to p-phenylenediamine in the presence of the new photocatalyst without the supplementary addition of a reducing agent (e.g., NaBH$_4$) in the reaction mixture. The catalytic reduction of 4-nitroaniline to p-phenylenediamine in the presence of Au–Ag photocatalyst with boronic acid moieties proceed with an apparent rate constant of k= 3.44×10^{-2} min^{-1} which is lower than for the system without boronic acid units but in the presence of NaBH$_4$ reducing agent (k = 23.34×10^{-2} min^{-1}). However, although the photocatalytic system needs to be improved, it can operate without an auxiliary reducing agent and can be repeatedly reused for up to six cycles with a significant decrease of the catalytic efficiency.

Palladium (Pd) nanoparticles or Pd-based complexes are one of the most efficient catalysts, extensively used in various organic reactions such as Mizoroki–Heck, Sonogashira, Stille, and Suzuki–Miyaura coupling reactions [131]. Moreover, the fabrication, characterization, and applications of polymer-supported Pd nanocatalysts and Pd complexes were recently reviewed [132], highlighting the advantages offered by the immobilization of Pd NPs in polymer matrices. However, there are still some drawbacks that have to be addressed (low reactivity of the catalysts at room temperature, need of high temperatures, or harsh reaction conditions), the reason that Chakraborty et al. [133] proposed the preparation of azobenzene-based colloidal porous organic polymer susceptible to a post-synthetic immobilization of metallic Pd nanocrystals for the preparation of visible and natural sunlight induced photocatalyst. To test the catalytic activity, Suzuki couplings of organohalides and phenylboronic acid derivatives under visible light or sunlight illumination were performed (Figure 10), observing the quantitative attaining of the desired products under mild reaction conditions. Moreover, the photocatalytic Suzuki coupling between phenyl iodide and phenylboronic acid in the presence of the projected catalyst was tested over ten successive recycling experiments, noting that there is no significant alteration of the catalytic efficiency. Given the fast reaction rate, the authors manufactured a prototype assembly with a continuous flow configuration controlled by pressure, achieving the reaction products in high yields.

The exciting results acquired in this study will certainly encourage scientists to design new efficient photocatalysts for a wide range of organic syntheses driven by visible light and sunlight as energy sources.
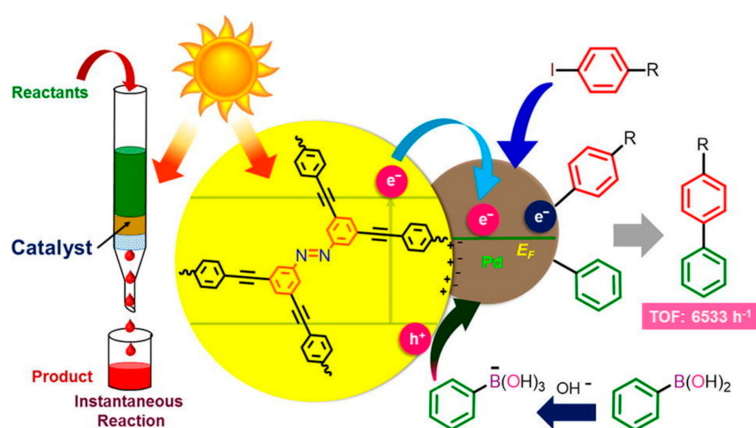
Figure 10. Schematic illustration of the mechanism of photocatalytic Suzuki coupling and of the continuous flow reaction setup. Reproduced by permission of Elsevier from [133].

6. Conclusions

In this review, a brief presentation of the latest achievements on hybrid photocatalytic materials prepared by a convenient combination of polymers and inorganic nanoparticles (metals or metal oxides) was accomplished. The great interest and advantages of using polymers as a support for different active inorganic photocatalysts, as well as the transition from conventional photocatalysts, such as TiO_2 and ZnO, active only in UV light, to more modern materials with higher potential to provide sunlight active photocatalysts such as CeO_2 and noble metal nanoparticles (Ag, Au, Pd) were emphasized. Various preparative methods used to obtain composite photocatalysts have been evaluated, highlighting the numerous synthetic pathways available for achieving high performance materials with tunable characteristics. In addition, the importance of replacing synthetic polymers derived from oil, gas, and carbon (non-renewable sources) whose availability is constantly decreasing with cheaper and more readily available polymeric matrices, such as biopolymers obtained from natural raw materials (chitosan, cellulose, xylan, etc.) is underlined. The main advantages offered by the use of polymer supports refer to the prevention of aggregation and release of the nanoparticles during the testing experiments, the easy recovery of the catalytic materials, and additionally, in the majority of the cases, the preservation or even improvement of the photocatalytic efficiency compared to the slurry systems. All photocatalytic systems described in this review are studied only under laboratory conditions, and for large-scale application they need to be thoroughly investigated, but however they are promising materials with many economic advantages: Stability, easily availability, low costs, and reusability. Therefore, we can affirm that polymer-based hybrid composites are a feasible "platform" for future photocatalytic devices.

Conflicts of Interest: The authors declare no conflict of interest.

References

1. Friehs, E.; AlSalka, Y.; Lavrentieva, A.; Jochums, A.; Walter, J.-G.; Stahl, F.; Scheper, T.; Bahnemann, D. Toxicity, phototoxicity and biocidal activity of nanoparticles employed in photocatalysis. *J. Photochem. Photobiol. C* **2016**, *29*, 1–28. [CrossRef]
2. Herrmann, J.M. Photocatalysis fundamentals revisited to avoid several misconceptions. *Appl. Catal. B Environ.* **2010**, *99*, 461–468. [CrossRef]
3. Yang, W.B.; Zhou, H.D.; Cicek, N. Treatment of organic micropollutants in water and or wastewater by UV-based processes: A literature review. *Crit. Rev. Environ. Sci. Technol.* **2014**, *44*, 1443–1476. [CrossRef]
4. Hashim, N.; Thakur, S.; Patang, M.; Crapulli, F.; Ray, A.K. Solar degradation of diclofenac using eosin-Y-activated TiO_2: Cost estimation, process optimization and parameter interaction study. *Environ. Technol.* **2016**, *38*, 1–12. [CrossRef] [PubMed]
5. Rahimi, R.; Zargari, S.; Yousefi, A.; Berijani, M.Y.; Ghaffarinejad, A.; Morsali, A. Visible light photocatalytic disinfection of E. Coli with TiO_2-graphene nanocomposite sensitized with tetrakis(4-carboxyphenyl)porphyrin. *Appl. Surf. Sci.* **2015**, *355*, 1098–1106. [CrossRef]
6. Albay, C.; Koç, M.; Altin, I.; Bayrak, R.; Degirmencioglu, I.; Sokmen, M. New dye sensitized photocatalysts: Copper(II)-phthalocyanine/TiO_2 nanocomposite for water remediation. *J. Photochem. Photobiol. A Chem.* **2016**, *324*, 117–125. [CrossRef]
7. Hemalatha, K.; Ette, P.M.; Madras, G.; Ramesha, K. Visible light assisted photocatalytic degradation of organic dyes on TiO2–CNT nanocomposites. *J. Sol-Gel Sci. Technol.* **2015**, *73*, 72–82. [CrossRef]
8. Badr, Y.; Mahmoud, M.A. Photocatalytic degradation of methyl orange by gold silver nano-core/silica nano-shell. *J. Phys. Chem. Solid* **2007**, *68*, 413–419. [CrossRef]
9. Zhao, X.; Lv, L.; Pan, B.; Zhang, W.; Zhang, S.; Zhang, Q. Polymer-supported nanocomposites for environmental application: A review. *Chem. Eng. J.* **2011**, *170*, 381–394. [CrossRef]
10. Mahouche-Chergui, S.; Guerrouache, M.; Carbonnier, B.; Chehimi, M.M. Polymer-immobilized nanoparticles. *Colloids Surf. A* **2013**, *439*, 43–68. [CrossRef]

11. Khanam, Z.; Sadon, N.A.; Adam, F. Synthesis and characterization of a novel paramagnetic polyaniline composite with uniformly distributed metallic nanoparticles sandwiched between polymer matrices. *Synth. Met.* **2014**, *192*, 1–9. [CrossRef]

12. Singh, S.; Mahalingam, H.; Singh, P.K. Polymer-supported titanium dioxide photocatalysts for environmental remediation: A review. *Appl. Catal. A Gen.* **2013**, *462*, 178–195. [CrossRef]

13. Colmenares, J.C.; Kuna, E. Photoactive hybrid catalysts based on natural and synthetic polymers: A comparative overview. *Molecules* **2017**, *22*, 790. [CrossRef] [PubMed]

14. Colmenares, J.C.; Varma, R.S.; Lisowski, P. Sustainable hybrid photocatalysts: Titania immobilized on carbon materials derived from renewable and biodegradable resources. *Green Chem.* **2016**, *18*, 5736–5750. [CrossRef]

15. Yu, H.; Shi, R.; Zhao, Y.; Bian, T.; Zhao, Y.; Zhou, C.; Waterhouse, G.I.N.; Wu, L.-Z.; Tung, C.-H.; Zhang, T. Alkali-assisted synthesis of nitrogen deficient graphitic carbon nitride with tunable band structures for efficient visible-light-driven hydrogen evolution. *Adv. Mater.* **2017**, *29*, 1605148. [CrossRef]

16. Kandavelu, V.; Kastien, H.; Thampi, K.R. Photocatalytic degradation of isothiazolin-3-ones in water and emulsion paints containing nanocrystalline TiO_2 and ZnO catalysts. *Appl. Catal. B Environ.* **2004**, *48*, 101–111. [CrossRef]

17. Ozgur, U.; Alivov, Y.I.; Liu, C.; Teke, A.; Reshchikov, M.; Dogan, S.; Avrutin, V.; Cho, S.-J.; Morkoc, H. A comprehensive review of ZnO materials and devices. *J. Appl. Phys.* **2005**, *98*, 041301. [CrossRef]

18. Ji, P.; Zhang, J.; Chen, F.; Anpo, M. Study of adsorption and degradation of Acid Orange 7 on the surface of CeO_2 under visible light irradiation. *Appl. Catal. B* **2009**, *85*, 148–154. [CrossRef]

19. Sarina, S.; Waclawik, E.R.; Zhu, H. Photocatalysis on supported gold and silver nanoparticles under ultraviolet and visible light irradiation. *Green Chem.* **2013**, *15*, 1814–1833. [CrossRef]

20. Xiao, Q.; Jaatinen, E.; Zhu, H. Direct photocatalysis for organic synthesis by using plasmonic-metal nanoparticles irradiated with visible light. *Chem. Asian J.* **2014**, *9*, 3046–3064. [CrossRef]

21. Yamada, K.; Miyajima, K.; Mafun, F. Thermionic emission of electrons from gold nanoparticles by nanosecond pulse-laser excitation of interband. *J. Phys. Chem. C* **2007**, *111*, 11246–11251. [CrossRef]

22. Fujishima, A.; Honda, K. Electrochemical photolysis of water at a semiconductor electrode. *Nature* **1972**, *238*, 37–38. [CrossRef] [PubMed]

23. Horiguchi, Y.; Kanda, T.; Torigoe, K.; Sakai, H.; Abe, M. Preparation of gold/silver/titania trilayered nanorods and their photocatalytic activities. *Langmuir* **2014**, *30*, 922–928. [CrossRef] [PubMed]

24. Li, X.; Wang, D.; Cheng, G.; Luo, Q.; An, J.; Wang, Y. Preparation of polyaniline-modified TiO_2 nanoparticles and their photocatalytic activity under visible light illumination. *Appl. Catal. B* **2008**, *81*, 267–273. [CrossRef]

25. Khataee, A.R.; Kasiri, M.B. Photocatalytic degradation of organic dyes in the presence of nanostructured titanium dioxide: Influence of the chemical structure of dyes. *J. Mol. Catal. Chem.* **2010**, *328*, 8–26. [CrossRef]

26. Nakata, K.; Fujishima, A. TiO_2 photocatalysis: Design and applications. *J. Photochem. Photobiol. C* **2012**, *13*, 169–189. [CrossRef]

27. Kasanen, J.; Salstela, J.; Suvanto, M.; Pakkanen, T.T. Photocatalytic degradation of methylene blue in water solution by multilayer TiO_2 coating on HDPE. *Appl. Surf. Sci.* **2011**, *258*, 1738–1743. [CrossRef]

28. He, Y.; Zhang, L.; Teng, B.; Fan, M. New application of Z-Scheme Ag_3PO_4/g-C_3N_4 composite in converting CO_2 to fuel. *Environ. Sci. Technol.* **2015**, *49*, 649–656. [CrossRef]

29. He, Y.; Wang, Y.; Zhang, L.; Teng, B.; Fan, M. High-efficiency conversion of CO_2 to fuel over ZnO/g-C_3N_4 photocatalyst. *Appl. Catal. B* **2015**, *168–169*, 1–8. [CrossRef]

30. Liu, L.C.; Gu, X.R.; Sun, C.Z.; Li, H.; Deng, Y.; Gao, F.; Dong, L. In situ loading of ultra-small Cu_2O particles on TiO_2 nanosheets to enhance the visible-light photoactivity. *Nanoscale* **2012**, *4*, 6351–6359. [CrossRef]

31. Zhu, J.F.; Deng, Z.G.; Chen, F.; Zhang, J.L.; Chen, H.J.; Anpo, M.; Huang, J.Z.; Zhang, L.Z. Hydrothermal doping method for preparation of Cr^{3+}-TiO_2 photocatalysts with concentration gradient distribution of Cr^{3+}. *Appl. Catal. B* **2006**, *62*, 329–335. [CrossRef]

32. Cha, W.; Le, H.A.; Chin, S.; Kim, M.; Jung, H.; Yun, S.-T.; Jurng, J. Enhanced low-temperature NH_3-SCR activity of a V_2O_5/TiO_2 composite prepared via chemical vapor condensation and impregnation method. *J. Mater. Res. Bull.* **2013**, *48*, 4415–4418. [CrossRef]

33. Li, Y.Z.; Jin, S.F.; Xie, H.; Chen, X.; Tian, T.T.; Zhao, X.J. Highly selective photocatalytic and sensing properties of 2D-ordered dome films of nano titania and nano Ag^{2+} doped titania. *J. Mater. Chem.* **2012**, *22*, 1469–1476. [CrossRef]

34. Chibac, A.L.; Melinte, V.; Buruiana, T.; Mangalagiu, I.; Buruiana, E.C. Preparation of photocrosslinked sol-gel composites based on urethane-acrylic matrix, silsesquioxane sequences, TiO$_2$, and Ag/Au Nanoparticles for use in photocatalytic applications. *J. Polym. Sci. Polym. Chem.* **2015**, *53*, 1189–1204. [CrossRef]

35. Naik, G.K.; Mishra, P.M.; Parida, K. Green synthesis of Au/TiO$_2$ for effective dye degradation in aqueous system. *Chem. Eng. J.* **2013**, *229*, 492–497. [CrossRef]

36. Ansari, S.A.; Khan, M.M.; Ansari, M.O.; Cho, M.H. Gold nanoparticles-sensitized wide and narrow band gap TiO$_2$ for visible light applications: A comparative study. *New J. Chem.* **2015**, *39*, 4708–4715. [CrossRef]

37. Pelaez, M.; Nolan, N.T.; Pillai, S.C.; Seery, M.K.; Falaras, P.; Kontos, A.G.; Dunlop, P.S.M.; Hamilton, J.W.J.; Byrne, J.A.; O'Shea, K.; et al. A review on the visible light active titanium dioxide photocatalysts for environmental applications. *Appl. Catal. B* **2012**, *125*, 331–349. [CrossRef]

38. Xu, Y.-J.; Zhuang, Y.; Fu, X. New insight for enhanced photocatalytic activity of TiO$_2$ by doping carbon nanotubes: A case study on degradation of benzene and methyl orange. *J. Phys. Chem. C* **2010**, *114*, 2669–2676. [CrossRef]

39. Wang, D.-H.; Jia, L.; Wu, X.-L.; Lu, L.-Q.; Xu, A.-W. One-step hydrothermal synthesis of N-doped TiO$_2$/C nanocomposites with high visible light photocatalytic activity. *Nanoscale* **2012**, *4*, 576–584. [CrossRef]

40. Tennakone, K.; Tilakaratne, C.T.K.; Kottegoda, I.R.M. Photocatalytic degradation of organic contaminants in water with TiO$_2$ supported on polythene films. *J. Photochem. Photobiol. A* **1995**, *87*, 177–179. [CrossRef]

41. Cámara, R.M.; Crespo, E.; Portela, R.; Suárez, S.; Bautista, L.; Gutiérrez-Martín, F.; Sánchez, B. Enhanced photocatalytic activity of TiO$_2$ thin films on plasma-pretreated organic polymers. *Catal. Today* **2014**, *230*, 145–151. [CrossRef]

42. Sadowski, R.; Wach, A.; Buchalska, M.; Kuśtrowski, P.; Macyk, W. Photosensitized TiO$_2$ films on polymers—Titania-polymer interactions and visible light induced photoactivity. *Appl. Surf. Sci.* **2019**, *475*, 710–719. [CrossRef]

43. Fischer, K.; Schulz, P.; Atanasov, I.; Latif, A.A.; Thomas, I.; Kühnert, M.; Prager, A.; Griebel, J.; Schulze, A. Synthesis of high crystalline TiO$_2$ nanoparticles on a polymer membrane to degrade pollutants from water. *Catalysts* **2018**, *8*, 376. [CrossRef]

44. Yang, C.; Han, N.; Zhang, W.; Wang, W.; Li, W.; Xia, B.; Han, C.; Cui, Z.; Zhang, X. Adhesive-free in situ synthesis of a coral-like titanium dioxide@poly(phenylene sulfide) microporous membrane for visible-light photocatalysis. *Chem. Eng. J.* **2019**, *374*, 1382–1393. [CrossRef]

45. Liu, Z.; Liu, R.; Yi, Y.; Han, W.; Kong, F.; Wang, S. Photocatalytic degradation of dyes over a xylan/PVA/TiO$_2$ composite under visible light irradiation. *Carbohydr. Polym.* **2019**, *223*, 115081. [CrossRef]

46. Shoueir, K.; Kandil, S.; El-hosainy, H.; El-Kemary, M. Tailoring the surface reactivity of plasmonic Au@TiO$_2$ photocatalyst bio-based chitosan fiber towards cleaner of harmful water pollutants under visible-light irradiation. *J. Clean. Prod.* **2019**, *230*, 383–393. [CrossRef]

47. Yu, J.; Pang, Z.; Zheng, C.; Zhou, T.; Zhang, J.; Zhou, H.; Wei, Q. Cotton fabric finished by PANI/TiO$_2$ with multifunctions of conductivity, anti-ultraviolet and photocatalysis activity. *Appl. Surf. Sci.* **2019**, *470*, 84–90. [CrossRef]

48. Malesic-Eleftheriadou, N.; Evgenidou, E.N.; Kyzas, G.Z.; Bikiaris, D.N.; Lambropoulou, D.A. Removal of antibiotics in aqueous media by using new synthesized bio-based poly(ethylene terephthalate)-TiO$_2$ photocatalysts. *Chemosphere* **2019**, *234*, 746–755. [CrossRef]

49. Sansotera, M.; Kheyli, S.G.M.; Baggioli, A.; Bianchi, C.L.; Pedeferri, M.P.; Diamanti, M.V.; Navarrini, W. Absorption and photocatalytic degradation of VOCs by perfluorinated ionomeric coating with TiO$_2$ nanopowders for air purification. *Chem. Eng. J.* **2019**, *361*, 885–896. [CrossRef]

50. Ayed, C.; Huang, W.; Li, R.; Caire da Silva, L.; Wang, D.; Suraeva, O.; Najjar, W.; Zhang, K.A.I. Conjugated microporous polymers with immobilized TiO$_2$ nanoparticles for enhanced visible light photocatalysis. *Part. Part. Syst. Charact.* **2018**, *35*, 1700234. [CrossRef]

51. Benhabiles, O.; Galiano, F.; Marino, T.; Mahmoudi, H.; Lounici, H.; Figoli, A. Preparation and characterization of TiO$_2$-PVDF/PMMA blend membranes using an alternative non-toxic solvent for UF/MF and photocatalytic application. *Molecules* **2019**, *24*, 724. [CrossRef]

52. Nakatani, H.; Hamachi, R.; Fukui, K.; Motokucho, S. Synthesis and activity characteristics of visible light responsive polymer photocatalyst system with a styrene block copolymer containing TiO$_2$ gel. *J. Colloid Interface Sci.* **2018**, *532*, 210–217. [CrossRef]

53.　Chibac, A.L.; Buruiana, T.; Melinte, V.; Mangalagiu, I.; Buruiana, E.C. Tuning the size and the photocatalytic performance of gold nanoparticles in situ generated in photopolymerizable glycomonomers. *RSC Adv.* **2015**, *5*, 90922–90931. [CrossRef]

54.　Chibac, A.L.; Buruiana, T.; Melinte, V.; Buruiana, E.C. Photocatalysis applications of some hybrid polymeric composites incorporating TiO_2 nanoparticles and their combinations with SiO_2/Fe_2O_3. *Beilstein J. Nanotechnol.* **2017**, *8*, 272–286. [CrossRef] [PubMed]

55.　Melinte, V.; Buruiana, T.; Rosca, I.; Chibac, A.L. TiO_2-based photopolymerized hybrid catalysts with visible light catalytic activity induced by in situ generated Ag/Au NPs. *ChemistrySelect* **2019**, *4*, 5138–5149. [CrossRef]

56.　Wei, Y.-Y.; Sun, X.-T.; Xu, Z.-R. One-step synthesis of bifunctional $PEGDA/TiO_2$ composite film by photopolymerization for the removal of Congo red. *Appl. Surf. Sci.* **2018**, *445*, 437–444. [CrossRef]

57.　Neghi, N.; Kumar, M.; Burkhalov, D. Synthesis and application of stable, reusable TiO_2 polymeric composites for photocatalytic removal of metronidazole: Removal kinetics and density functional analysis. *Chem. Eng. J.* **2019**, *359*, 963–975. [CrossRef]

58.　Bergamonti, L.; Bergonzi, C.; Graiff, C.; Lottici, P.P.; Bettini, R.; Elviri, L. 3D printed chitosan scaffolds: A new TiO_2 support for the photocatalytic degradation of amoxicillin in water. *Water Res.* **2019**, *163*, 114841. [CrossRef]

59.　Gu, L.; Wang, J.; Qi, R.; Wang, X.; Xu, P.; Han, X. A novel incorporating style of polyaniline/TiO_2 composites as effective visible photocatalysts. *J. Mol. Catal. Chem.* **2012**, *357*, 19–25. [CrossRef]

60.　Wang, J.; Ni, X. Photoresponsive polypyrrole-TiO_2 nanoparticles film fabricated by a novel surface initiated polymerization. *Solid State Commun.* **2008**, *146*, 239–244. [CrossRef]

61.　Wang, F.; Min, S.X. TiO_2/polyaniline composites: An efficient photocatalyst for the degradation of methylene blue under natural light. *Chin. Chem. Lett.* **2007**, *8*, 1273–1277. [CrossRef]

62.　Lee, S.L.; Chang, C.J. Recent developments about conductive polymer based composite photocatalysts. *Polymers* **2019**, *11*, 206. [CrossRef] [PubMed]

63.　Riaz, U.; Ashraf, S.M.; Kashyap, J. Role of conducting polymers in enhancing TiO_2-based photocatalytic dye degradation: A short review. *Polym. Plast. Technol.* **2015**, *54*, 1850–1870. [CrossRef]

64.　Reddy, K.R.; Karthik, K.V.; Prasad, S.B.B.; Soni, S.K.; Jeong, H.M.; Raghu, A.V. Enhanced photocatalytic activity of nanostructured titanium dioxide/polyaniline hybrid photocatalysts. *Polyhedron* **2016**, *120*, 169–174. [CrossRef]

65.　Zhao, J.; Biswas, M.R.U.D.; Oh, W.C. A novel $BiVO_4$-GO-TiO_2-PANI composite for upgraded photocatalytic performance under visible light and its non-toxicity. *Environ. Sci. Pollut. Res.* **2019**, *26*, 11888–11904. [CrossRef] [PubMed]

66.　Sangareswari, M.; Meenakshi Sundaram, M. Development of efficiency improved polymer-modified TiO_2 for the photocatalytic degradation of an organic dye from wastewater environment. *Appl. Water Sci.* **2017**, *7*, 1781–1790. [CrossRef]

67.　Krehula, L.K.; Stjepanović, J.; Perlog, M.; Krehula, S.; Gilja, V.; Travas-Sejdic, J.; Hrnjak-Murgić, Z. Conducting polymer polypyrrole and titanium dioxide nanocomposites for photocatalysis of RR45 dye under visible light. *Polym. Bull.* **2019**, *76*, 1697–1715. [CrossRef]

68.　Moniz, S.J.A.; Shevlin, S.A.; Martin, D.J.; Guo, Z.X.; Tang, J.W. Visible-light driven heterojunction photocatalysts for water splitting-a critical review. *Energy Environ. Sci.* **2015**, *8*, 731–759. [CrossRef]

69.　Yang, L.; Yu, Y.; Zhang, J.; Chen, F.; Meng, X.; Qiu, Y.; Dan, Y.; Jiang, L. In-situ fabrication of diketopyrrolopyrrole-carbazole-based conjugated polymer/TiO_2 heterojunction for enhanced visible light photocatalysis. *Appl. Surf. Sci.* **2018**, *434*, 796–805. [CrossRef]

70.　Che, J.; Bae, N.; Noh, J.; Kim, T.; Yoo, P.J.; Shin, T.J.; Park, J. Poly(3-hexylthiophene) nanoparticles prepared via a film shattering process and hybridization with TiO_2 for visible-light active photocatalysis. *Macromol. Res.* **2016**, *27*, 427–434. [CrossRef]

71.　Yang, C.X.; Dong, W.P.; Cui, G.W.; Zhao, Y.Q.; Shi, X.F.; Xia, X.Y.; Tang, B.; Wang, W.L. Highly-efficient photocatalytic degradation of methylene blue by PoPD-modified TiO_2 nanocomposites due to photosensitization-synergetic effect of TiO_2 with PoPD. *Sci. Rep.* **2017**, *7*, 3973. [CrossRef] [PubMed]

72.　Samadi, M.; Zirak, M.; Naseri, A.; Khorashadizade, E.; Moshfegh, A.Z. Recent progress on doped ZnO nanostructures for visible-light photocatalysis. *Thin Solid Films* **2016**, *605*, 2–19. [CrossRef]

73.　Janotti, A.; Van de Walle, C.G. Fundamentals of zinc oxide as a semiconductor. *Rep. Prog. Phys.* **2009**, *72*, 126501. [CrossRef]

74. Peng, W.Q.; Qu, S.C.; Cong, G.W.; Wang, Z.G. Structure and visible luminescence of ZnO nanoparticles. *Mater. Sci. Semicond. Process.* **2006**, *9*, 156–159. [CrossRef]

75. Anandan, S.; Ohashi, N.; Miyauchi, M. ZnO-based visible-light photocatalyst: Band-gap engineering and multi-electron reduction by co-catalyst. *Appl. Catal. B Environ.* **2010**, *100*, 502–509. [CrossRef]

76. Hasnat, M.A.; Uddin, M.M.; Samed, A.; Alam, S.S.; Hossain, S. Adsorption and photocatalytic decolorization of a synthetic dye erythrosine on anatase TiO$_2$ and ZnO surfaces. *J. Hazard. Mater.* **2007**, *147*, 471–477. [CrossRef]

77. Peternel, I.; Koprivanac, N.; Kusic, H. UV-based processes for reactive azo dye mineralization. *Water Res.* **2006**, *40*, 525–532. [CrossRef]

78. Ahangar, E.G.; Abbaspour-Fard, M.H.; Shahtahmassebi, N.; Khojastehpour, M.; Maddahi, P. Preparation and characterization of PVA/ZnO nanocomposite. *J. Food Process Pres.* **2015**, *39*, 1442–1451. [CrossRef]

79. Liang, S.; Xiao, K.; Mo, Y.; Huang, X. A novel ZnO nanoparticle blended polyvinylidene fluoride membrane for anti-irreversible fouling. *J. Memb. Sci.* **2012**, *394*, 184–192. [CrossRef]

80. Daneshvar, N.; Salari, D.; Khataee, A.R. Photocatalytic degradation of azo dye acid red 14 in water on ZnO as an alternative catalyst to TiO$_2$. *J. Photochem. Photobiol. A* **2004**, *162*, 317–322. [CrossRef]

81. Herrmann, J.-M. Heterogeneous photocatalysis: Fundamentals and applications to the removal of various types of aqueous pollutants. *Catal. Today* **1999**, *53*, 115–129. [CrossRef]

82. Sivasankari, J.; Sankar, S.; Selvakumar, S.; Vimaladevi, L.; Krithiga, R. Synthesis, structural and optical properties of Er doped, Li doped and Er + Li co-doped ZnO nanocrystallites by solution-combustion method. *Mater. Chem. Phys.* **2014**, *143*, 1528–1535. [CrossRef]

83. Muthulingam, S.; Bae, K.B.; Khan, R.; Lee, I.H.; Periyayya, U. Improved daylight-induced photocatalytic performance and suppressed photocorrosion of N-doped ZnO decorated with carbon quantum dots. *RSC Adv.* **2015**, *5*, 46247–46251. [CrossRef]

84. Chen, T.; Yu, S.W.; Fang, X.X.; Huang, H.H.; Li, L.; Wang, X.Y.; Wang, H.H. Enhanced photocatalytic activity of C@ZnO core-shell nanostructures and its photoluminescence property. *Appl. Surf. Sci.* **2016**, *389*, 303–310. [CrossRef]

85. Udawatte, N.; Lee, M.; Kim, J.; Lee, D. Well-Defined Au/ZnO Nanoparticle Composites Exhibiting Enhanced Photocatalytic Activities. *ACS Appl. Mater. Interfaces* **2011**, *3*, 4531–4538. [CrossRef]

86. Carina, B.; Judith, S.; Thomas, M.; Thomas, L.; Daniel, R.W.; Andreas, G.; Josef, B.; Holger, S. Mesostructured ZnO/Au nanoparticle composites with enhanced photocatalytic activity. *Polymer* **2017**, *128*, 65–70. [CrossRef]

87. Pant, H.R.; Pant, B.; Kim, H.J.; Amarjargal, A.; Park, C.H.; Tijing, L.D.; Kim, E.K.; Kim, C.S. A green and facile one-pot synthesis of Ag-ZnO/RGO nanocomposite with effective photocatalytic activity for removal of organic pollutants. *Ceram. Int.* **2013**, *39*, 5083–5091. [CrossRef]

88. Podasca, V.E.; Buruiana, T.; Buruiana, E.C. UV-cured polymeric films containing ZnO and silver nanoparticleswith UV–vis light-assisted photocatalytic activity. *Appl. Surf. Sci.* **2016**, *377*, 262–273. [CrossRef]

89. Chougule, M.A.; Sen, S.; Patil, V.B. Facile and efficient route for preparation of polypyrrole-ZnO nanocomposites: Microstructural, optical, and charge transport properties. *J. Appl. Polym. Sci.* **2012**, *125*, E541–E547. [CrossRef]

90. Kayaci, F.; Vempati, S.; Ozgit-Akgun, C.; Donmez, I.; Biyikli, N.; Uyar, T. Transformation of polymer-ZnO core–shell nanofibers into ZnO hollow nanofibers: Intrinsic defect reorganization in ZnO and its influence on the photocatalysis. *Appl. Catal. B Environ.* **2015**, *176–177*, 646–653. [CrossRef]

91. Schwartz, V.B.; Thétiot, F.; Ritz, S.; Pütz, S.; Choritz, L.; Lappas, A.; Förch, R.; Landfester, K.; Jonas, U. Antibacterial surface coatings from zinc oxide nanoparticles embedded in poly(N-isopropylacrylamide) hydrogel surface layers. *Adv. Funct. Mater.* **2012**, *22*, 2376–2386. [CrossRef]

92. Yuan, X.; Xu, W.; Huang, F.; Chen, D.; Wei, Q. Polyester fabric coated with Ag/ZnO composite film by magnetron sputtering. *Appl. Surf. Sci.* **2016**, *390*, 863–869. [CrossRef]

93. Nicolay, A.; Lanzutti, A.; Poelman, M.; Ruelle, B.; Fedrizzi, L.; Dubois, P.; Olivier, M.-G. Elaboration and characterization of a multifunctional silane/ZnO hybrid nanocomposite coating. *Appl. Surf. Sci.* **2015**, *327*, 379–388. [CrossRef]

94. Todorova, N.; Giannakopoulou, T.; Pomoni, K.; Yu, J.; Vaimakis, T.; Trapalis, C. Photocatalytic NOx oxidation over modified ZnO/TiO$_2$ thin films. *Catal. Today* **2015**, *252*, 41–46. [CrossRef]

95. Qin, R.; Hao, L.; Liu, Y.; Zhang, Y. Polyaniline-ZnO hybrid nanocomposites with enhanced photocatalytic and electrochemical performance. *ChemistrySelect* **2018**, *3*, 6286–6293. [CrossRef]

96. Ameen, S.; Akhtar, M.S.; Kim, Y.S.; Yang, O.-B.; Shin, H.-S. An effective nanocomposite of polyaniline and ZnO: Preparation, characterizations, and its photocatalytic activity. *Colloid Polym. Sci.* **2011**, *289*, 415–421. [CrossRef]

97. Eskizeybek, V.; Sari, F.; Gülce, H.; Gülce, A.; Avci, A. Preparation of the new polyaniline/ZnO nanocomposite and its photocatalytic activity for degradation of methylene blue and malachite green dyes under UV and natural sun lights irradiations. *Appl. Catal. B* **2012**, *119*, 197–206. [CrossRef]

98. Saravanan, R.; Sacari, E.; Gracia, F.; Khan, M.M.; Mosquera, E.; Gupta, V.K. Conducting PANI stimulated ZnO system for visible light photocatalytic degradation of coloured dyes. *J. Mol. Liq.* **2016**, *221*, 1029–1033. [CrossRef]

99. Asgari, E.; Esrafilia, A.; Jafaria, A.J.; Kalantarya, R.R.; Nourmoradic, H.; Farzadkia, M. The comparison of ZnO/polyaniline nanocomposite under UV and visible radiations for decomposition of metronidazole: Degradation rate, mechanism and mineralization. *Process Saf. Environ.* **2019**, *128*, 65–76. [CrossRef]

100. Silvestri, S.; Ferreira, C.D.; Oliveira, V.; Varejão, J.M.T.B.; Labrincha, J.A.; Tobaldi, D.M. Synthesis of PPy-ZnO composite used as photocatalyst for the degradation of diclofenac under simulated solar irradiation. *J. Photochem. Photobiol. A* **2019**, *375*, 261–269. [CrossRef]

101. Ding, Q.; Miao, Y.E.; Liu, T. Morphology and photocatalytic property of hierarchical polyimide/ZnO fibers prepared via a direct ion-exchange process. *ACS Appl. Mater. Interfaces* **2013**, *512*, 5617–5622. [CrossRef] [PubMed]

102. Di Mauro, A.; Cantarella, M.; Nicotra, G.; Pellegrino, G.; Gulino, A.; Brundo, M.V.; Privitera, V.; Impellizzeri, G. Novel synthesis of ZnO/PMMA nanocomposites for photocatalytic applications. *Sci. Rep.* **2017**, *7*, 40895. [CrossRef] [PubMed]

103. Rani, M.; Shanker, U. Sun-light driven rapid photocatalytic degradation of methylene blue by poly(methyl methacrylate)/metal oxide nanocomposites. *Colloids Surf. A* **2018**, *559*, 136–147. [CrossRef]

104. Lefatshe, K.; Muiva, C.M.; Kebaabetswe, L.P. Extraction of nanocellulose and in-situ casting of ZnO/cellulose nanocomposite with enhanced photocatalytic and antibacterial activity. *Carbohydr. Polym.* **2017**, *164*, 301–308. [CrossRef]

105. Ibhandon, A.O.; Fitzpatrick, P. Heterogeneous photocatalysis: Recent advances and applications. *Catalysts* **2013**, *3*, 189–218. [CrossRef]

106. Rajeswari, A.; Christy, E.J.S.; Pius, A. New insight of hybrid membrane to degrade Congo red and Reactive yellow under sunlight. *J. Photochem. Photobiol. B* **2018**, *179*, 7–17. [CrossRef]

107. Ussia, M.; Di Mauro, A.; Mecca, T.; Cunsolo, F.; Cerruti, P.; Nicotra, G.; Spinella, C.; Impellizzeri, G.; Privitera, V.; Carroccio, S.C. ZnO-pHEMA nanocomposites: An eco-friendly and reusable material for water remediation. *ACS Appl. Mater. Interfaces* **2018**, *10*, 40100–40110. [CrossRef]

108. Ghanem, A.F.; Badawy, A.A.; Mohram, M.E.; Abdelrehim, M.H. Enhancement the photocatalytic and biological activity of nano-sized ZnO using hyperbranched polyester. *J. Inorg. Orgmet. Polym. Mater.* **2019**, *29*, 928–938. [CrossRef]

109. Ghanem, A.F.; Badawy, A.A.; Ismail, N.; Tian, Z.R.; Rehim, M.H.A.; Rabia, A. Photocatalytic activity of hyperbranched polyester/TiO₂ nanocomposites. *Appl. Catal. A* **2014**, *472*, 191–197. [CrossRef]

110. Campagnolo, L.; Lauciello, S.; Athanassiou, A.; Fragouli, D. Au/ZnO hybrid nanostructures on electrospun polymeric mats for improved photocatalytic degradation of organic pollutants. *Water* **2019**, *11*, 1787. [CrossRef]

111. Arslan, O.; Topuz, F.; Eren, H.; Biyikli, N.; Uyar, T. Pd nanocube decoration onto flexible nanofibrous mats of core-shell polymer-ZnO nanofibers for visible light photocatalysis. *New J. Chem.* **2017**, *41*, 4145–4156. [CrossRef]

112. Podasca, V.E.; Buruiana, T.; Buruiana, E.C. Photocatalytic degradation of Rhodamine B dye by polymeric films containing ZnO, Ag nanoparticles and polypyrrole. *J. Photochem. Photobiol. A* **2019**, *371*, 188–195. [CrossRef]

113. Sarro, M.; Gule, N.P.; Laurenti, E.; Gamberini, R.; Paganini, M.P.; Mallon, P.E.; Calza, P. ZnO-based materials and enzymes hybrid systems as highly efficient catalysts for recalcitrant pollutants abatement. *Chem. Eng. J.* **2018**, *334*, 2530–2538. [CrossRef]

114. Ansari, S.A.; Khan, M.M.; Ansari, M.O.; Kalathil, S.; Lee, J.; Cho, M.H. Band gap engineering of CeO₂ nanostructure by electrochemically active biofilm for visible light applications. *RSC Adv.* **2014**, *4*, 16782–16791. [CrossRef]

115. Ma, Y.Y.; Gao, W.; Zhang, Z.Y.; Zhang, S.; Tian, Z.M.; Liu, Y.X.; Ho, J.C.; Qu, Y.Q. Regulating the surface of nanoceria and its applications in heterogeneous catalysis. *Surf. Sci. Rep.* **2018**, *73*, 1–36. [CrossRef]

116. Sims, C.M.; Maier, R.A.; Johnston-Peck, A.C.; Gorham, J.M.; Hackley, V.A.; Nelson, B.C. Approaches for the quantitative analysis of oxidation state in cerium oxide nanomaterials. *Nanotechnology* **2019**, *30*, 085703. [CrossRef] [PubMed]

117. Ni, X.J.; Zhang, J.F.; Hong, L.; Yang, C.; Li, Y.X. Reduced graphene oxide@ceria nanocomposite-coated polymer microspheres as a highly active photocatalyst. *Colloids Surf. A* **2019**, *567*, 161–170. [CrossRef]

118. Oriekhova, O.; Le Coustumer, P.; Stoll, S. Impact of biopolymer coating on the colloidal stability of manufactured CeO_2 nanoparticles in contrasting water conditions. *Colloids Surf. A* **2017**, *533*, 267–274. [CrossRef]

119. Aguirre, M.; Salazar-Sandoval, E.J.; Johansson, M.; Ahniyaz, A.; Paulis, M.; Leiza, J.R. Hybrid acrylic/CeO_2 nanocomposites using hydrophilic, spherical and high aspect ratio CeO_2 nanoparticles. *J. Mater. Chem. A* **2014**, *2*, 20280–20287. [CrossRef]

120. Salazar-Sandoval, E.J.; Aguirre, M.; Paulis, M.; Leiza, J.R.; Johansson, M.; Ahniyaz, A. Radical initiator modified cerium oxide nanoparticles for polymer encapsulation via grafting from the surface. *RSC Adv.* **2014**, *4*, 61863–61868. [CrossRef]

121. Martin-Fabiani, I.; Koh, M.L.; Dalmas, F.; Elidottir, K.L.; Hinder, S.J.; Jurewicz, I.; Lansalot, M.; Bourgeat-Lami, E.; Keddie, J.L. Design of waterborne nanoceria/polymer nanocomposite UV-absorbing coatings: Pickering versus blended particles. *ACS Appl. Nano Mater.* **2018**, *1*, 3956–3968. [CrossRef]

122. Fischer, V.; Lieberwirth, I.; Jakob, G.; Landfester, K.; Muñoz-Espí, R. Metal oxide/polymer hybrid nanoparticles with versatile functionality prepared by controlled surface crystallization. *Adv. Funct. Mater.* **2013**, *23*, 451–466. [CrossRef]

123. Morselli, D.; Campagnolo, L.; Prato, M.; Papadopoulou, E.L.; Scarpellini, A.; Athanassiou, A.; Fragouli, D. Ceria/gold nanoparticles in situ synthesized on polymeric membranes with enhanced photocatalytic and radical scavenging activity. *ACS Appl. Nano Mater.* **2018**, *1*, 5601–5611. [CrossRef]

124. Peiris, S.; McMurtrie, J.; Zhu, H.Y. Metal nanoparticle photocatalysts: Emerging processes for green organic synthesis. *Catal. Sci. Technol.* **2016**, *6*, 320–338. [CrossRef]

125. Saeed, K.; Khan, I.; Shah, T.; Park, S.Y. Synthesis, characterization and photocatalytic activity of silver nanoparticles/amidoxime-modified polyacrylonitrile nanofibers. *Fibers Polym.* **2015**, *16*, 1870–1875. [CrossRef]

126. Jana, B.; Bhattacharyya, S.; Patra, A. Conjugated polymer P3HT/Au hybrid nanostructure for enhancing photocatalytic activity. *Phys. Chem. Chem. Phys.* **2015**, *17*, 15392–15399. [CrossRef]

127. Ghosh, S.; Mallik, A.K.; Basu, R.N. Enhanced photocatalytic activity and photoresponse of poly(3,4-ethylenedioxythiophene) nanofibers decorated with gold nanoparticle under visible light. *Sol. Energy* **2018**, *159*, 548–560. [CrossRef]

128. Abu Bakar, N.H.H.; Jamil, N.I.F.; Tan, W.L.; Sabri, N.A.; Tan, T.-W.; Abu Bakar, M. Environmental friendly natural rubber-blend-poly-vinylpyrrolidone/silver (NR-b-PVP/Ag) films for improved solar driven degradation of organic pollutants at neutral pH. *J. Photochem. Photobiol. A* **2018**, *352*, 9–18. [CrossRef]

129. Hareesh, K.; Sunitha, D.V.; Dhamgaye, V.P.; Dhole, S.D.; Bhoraskar, V.N.; Phase, D.M. Synchrotron X-ray radiation assisted synthesis of Ag/polycarbonate and Au/polycarbonate polymer matrix and its pollutant degradation application. *Nucl. Instrum. Meth. B* **2019**, *447*, 100–106. [CrossRef]

130. Melinte, V.; Stroea, L.; Buruiana, T.; Chibac, A.L. Photocrosslinked hybrid composites with Ag, Au or Au-Ag NPs as visible light triggered photocatalysts for degradation/reduction of aromatic nitroderivatives. *Eur. Polym. J.* **2019**, *121*, 109289. [CrossRef]

131. Phan, N.T.S.; Van Der Sluys, M.; Jones, C.W. On the nature of the active species in palladium catalyzed Mizoroki-Heck and Suzuki-Miyaura couplings–homogeneous or heterogeneous catalysis, a critical review. *Adv. Synth. Catalys.* **2006**, *348*, 609–679. [CrossRef]

132. Nasrollahzadeh, M.; Sajjadi, M.; Shokouhimehr, M.; Varma, R.S. Recent developments in palladium (nano)catalysts supported on polymers for selective and sustainable oxidation processes. *Coord. Chem. Rev.* **2019**, *397*, 54–75. [CrossRef]

133. Chakraborty, J.; Nath, I.; Verpoort, F. Pd-nanoparticle decorated azobenzene based colloidal porous organic polymer for visible and natural sunlight induced Mott-Schottky junction mediated instantaneous Suzuki coupling. *Chem. Eng. J.* **2019**, *358*, 580–588. [CrossRef]